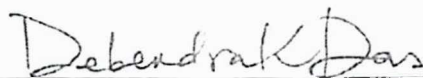# TESTING AND ANALYSIS OF A GROUND SOURCE HEAT PUMP IN INTERIOR ALASKA

By

Robbin Garber-Slaght

RECOMMENDED: _____
Dr. Debendra Das
Advisory Committee Co-Chair

_____
Dr. Tom Marsik
Advisory Committee Co-Chair

_____
Dr. Chuen-Sen Lin
Advisory Committee Member

_____
Dr. Rorik Peterson
Chair, Department of Mechanical Engineering

APPROVED: _____
Dean, College of Engineering and Mines

_____
Dean of the Graduate School

_____
Date   8/14/17

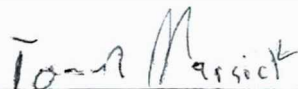TESTING AND ANALYSIS OF A GROUND SOURCE HEAT PUMP IN INTERIOR
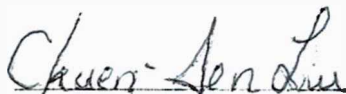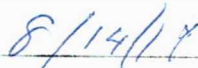
ALASKA

By

Robbin Garber-Slaght, B.A. M.L.I.S, B.S.

A Thesis Submitted in Partial Fulfillment of the Requirements

for the Degree of

Masters of Science

in

Cold Climate Engineering: Interdisciplinary Program

University of Alaska Fairbanks

August 2019

APPROVED:

Debendra K. Das, Committee Co-Chair
Tomas Marsik, Co-Chair
Chuen-Sen Lin, Committee Member
Rorik Peterson, Chair
    Department of Mechanical Engineering
William Schnabel, Dean
    College of Engineering and Mines
Michael Castellini, *Dean of the Graduate School*

Abstract

Ground source heat pumps (GSHPs) can be an efficient heating and cooling system in much of the world. However, their ability to work in extreme cold climates is not well studied. In a heating-dominated cold climate, the heat extracted from the soil is not actively replaced in the summer because there is very little space cooling. A ground source heat pump was installed at the Cold Climate Housing Research Center (CCHRC) in Fairbanks, Alaska with the intent to collect data on its performance and effects on the soil for at least ten years.

Analysis shows GSHPs are viable in the Fairbanks climate; however, their performance may degrade over time. According to two previous finite element models, the CCHRC heat pump seems to reach equilibrium in the soil at a COP of about 2.5 in five to seven years. Data from the first four heating seasons of the ground source heat pump at CCHRC is evaluated. The efficiency of the heat pump degraded from an average coefficient of performance (COP) of 3.7 to a mediocre 2.8 over the first four heating seasons.

Nanofluids are potential heat transfer fluids that could be used to enhance the heat transfer in the ground heat exchanger. Improved heat transfer could lower installation costs by making the ground heat exchanger smaller. A theoretical analysis of adding nanoparticles to the fluid in the ground heat exchanger is conducted. Two nanofluids are evaluated to verify improved heat transfer and potential performance of the heat pump system.

Data from the CCHRC heat pump system has also been used to analyze a 2-dimensional finite element model of the system's interaction with the soil. A model based on the first four years of data is developed using Temp/W software evaluates the ground heat exchanger for a thirty-year period. This model finds that the ground heat exchanger does not lower the ground temperature in the long term.

Acknowledgements

I would like to thank my committee co-chair Dr. Debendra Das for his support, knowledge and encouragement through this long process. I would also like to thank my committee members Dr. Tom Marsik (co-chair) and Dr. Chuen-Sen Lin for their guidance in completing this thesis.

Thank you also to all of my co-workers at the Cold Climate Housing Research Center who have advised and helped with many aspects of this project. Thanks to my many collaborators on this project: Dr. Rorik Peterson, Dr. Ronnie Daanen, Dr. John Zarling, Dr. Jeffery Spitler, Andy Roe, Colin Craven, Dustin Madden and Vanessa Stevens.

And finally, special thanks to my husband, Chris, who has been my greatest supporter in this long quest.

Table of Contents

List of Figures

List of Tables

Chapter 1: Thesis Introduction

1.1 Introduction

Ground source heat pumps (GSHPs) are used around the world for space conditioning. They rely on a large energy sink (usually soil or a large water body) for heat rejection or extraction. In climates with balanced heating and cooling demand GHSPs work well because energy is rejected to and collected from the ground sink on an equal basis. In colder climates that do not have cooling demands GHSPs extract much more energy from the ground than is returned. This unbalanced energy extraction lowers the temperature of the ground and thus the efficiency of the heat pump. Analysis of GSHPs performance in cold climates over multiple heating seasons had not been studied prior to the beginning of this research. In 2013 a GSHP was installed at the Cold Climate Housing Research Center (CCHRC) in Fairbanks, Alaska with the intent to collect data on its performance and effects on the soil for at least 10 years.

The demonstration GSHP at CCHRC provides a wealth of data on a system that is at the edge of the recommended range for heat pumps and in a marginal location. The unfrozen ground temperature in this location is approximately 1°C and there is frozen soil (near 0°C) at approximately 9.5 m below the surface. The GSHP project has been presented in some conference proceedings and journals [1]–[3]. The CCHRC heat pump system data has been used to inform several computer models of the soil around the ground heat exchanger (GHE).

In addition to data on this particular installation, the GSHP data is being utilized in this thesis to look at alternative GHE fluids. These alternative fluids, called nanofluids, have suspended particles that are 100 nm or less in diameter and can enhance the thermal conductivity of the fluid. There are several different types of nanoparticles; this thesis focuses on alumina (Al_2O_3) and copper oxide (CuO). The base fluid for this analysis is 20:80 methanol/water, which is the GHE fluid of the CCHRC heat pump system.

1.2 Cold Climate Ground Source Heat Pumps - Literature Review

CCHRC and the Alaska Center for Energy and Power (ACEP) completed a study on ground source heat pump technology in cold climates in 2011 [4]. They found that, depending on the system performance, the price of oil, and available rebates, GSHPs can be cost effective in many areas in Alaska even with high capital costs. The study also found that the use of GSHPs is increasing in colder climates as the technology improves, but there is a lack of information on

long-term performance in cold climates. Of particular interest is the effect of unbalanced heat extraction on the soil surrounding the GHE and the potential degradation in the efficiency of the heat pump system. Heat extraction from the ground that does not have equal heat recharge by GSHP space cooling and solar radiation in the summer months has the potential to increase permafrost, especially in areas with existing discontinuous permafrost.

A few studies have looked at ways to achieve better GSHP performance in heating dominated climates. Wu, et al. [5] note that the soil temperatures around a GHE in a heating dominated climate can degrade over time, which reduces the efficiency of the GSHP. There are several approaches to overcoming this problem: increasing the GHE size, installing a secondary heating source, and using thermal storage [5]. You, et al. [6] also suggest several ways to improve GHE performance. Increasing the size of the GHE or changing the layout of boreholes can mitigate thermal imbalance slightly, but is not effective for a larger thermal imbalance. Modifying the heat pump system itself to include auxiliary heating sources or restricting use to certain times of the day when other heating options are not available is a practical and effective way to help the GHE maintain higher temperatures and improves efficiency [6].

Eslami-nejad and Bernier [7] found that by saturating soils around the GHE boreholes, latent energy from freezing the soil was added to the heat pump system. Yang, et al. [8] also looked at phase change process in the GHE. They found that freezing in the GHE area can enhance the heat transfer performance and can help in downsizing the heat exchanger. The higher thermal diffusivity of the soil has the largest effect on the improvement of heat transfer with phase change in the heat exchanger [8]. Vasil'ev, et al. [9] developed a computational model to study the effects of latent heat on a borehole heat pump installations. They determined that low moisture soils will create a larger freeze radius around the boreholes than high moisture soils. Additionally, an analysis of phase change is critical for any models of heat pumps in heating dominated climates [9].

Rezaei, et al. [10] studied the effects of surface treatments on soil temperatures in a GHE. A layer of tire-derived aggregate (shredded tires) affected soil temperatures down to 4 m with a layer of material that is 0.2 m thick [10]. The surface layer of aggregate had the potential to increase the energy absorbed from the "GHE by 17% over no surface treatment" and the aggregate performed better in cold climates [10].

Zhihua et al. [11] studied a long-running vertical GHE heat pump in Tianjin, China to

2

evaluate the thermal imbalance on the soil temperatures. Tianjin is a cooling dominated climate but their analysis of the thermal imbalance is instructive to both heating and cooling dominated climates. The cooling load was approximately twice the heating load in this study. They found the imbalance led to a gradual increase in soil temperature and at 30 years expect an auxiliary cooling unit will be required [11] due to the loss of cooling capacity in the soil.

Bakirci [12] evaluated an experimental vertical GHE heat pump in Erzurum, Turkey. While warmer than Fairbanks, Alaska, Erzurum is one of the colder climates where heat pumps have been evaluated, the average January temperature is -10.8 °C and the annual minimum temperature is -16.9°C while the annual maximum is 17.3°C. Bakirici's study was only over one winter and he found the system was effective with a COP of 3.0 to 2.6 in the coldest months [12].

As Meyer et al. found there are very few long-term studies of heat pumps in cold climates. Prior to this CCHRC study, the longest study of the GSHP as a heating source in Alaska lasted 1.5 years and concluded that the soil temperatures with the GHE at 1.2 m of depth recovered early in the summer season [13]. A one-year study in South-central Alaska found that deeper heat extraction coils (2.7 m) did not recover temperature completely in the summer months, whereas the shallower coils (1.5 m) recovered well [14].

The longest cold climate heat pump studies use heat pumps to cool building foundations to protect the permafrost. Svalbard, Norway has several buildings that use heat pump cooling to maintain the permafrost [15]. A 1993 home retrofit in Fairbanks installed a GSHP under the foundation to re-cool the permafrost and maintained the foundation for more than 20 years [16]. Neither of these studies looked into the performance of the heat pump as a space heating device.

1.3 Nanofluids – Literature Review

Applying the advances in nanotechnology to heat transfer in the rather new field of nanofluids has only been around since in the mid-1990s. Nanofluids research studies the addition of nano sized particles (usually less than 100 nm [17]) to heat transfer fluids so that there is an improvement in thermal transfer properties of the new nanofluid. Since these are new liquids with unique properties much of the research to date has been toward defining their thermal properties. This project looks at nanofluids with the assumption of Newtonian behavior, although Namburu et al. [18] and Sahoo et al. [19] found that some nanofluids display non-Newtonian behavior at low temperature. Sahoo et al. [19] found that Al_2O_3 in concentrations up to 10% in

3

60:40 EG/W base fluid behaved like a non-Newtonian fluid below 0°C and as a Newtonian fluid above 0°C.

Nanofluids are a combination of a base fluid and a nano sized particle. Much research has been done on water as a base fluid; more recent research has looked at ethylene glycol, propylene glycol, and methanol base fluids. These base fluids can be combined with one of an ever increasing list of nanoparticles: alumina (Al_2O_3), copper oxide (CuO), titanium dioxide (TiO_2), copper (Cu), zinc oxide (ZnO), silicon dioxide (SiO_2), and carbon nanotubes. Each base fluid and nanoparticle combination will have different thermal properties.

In addition to the variation in combinations, the concentration of nanoparticles in the base fluid also has significant impact on thermal properties. Research has looked at volumetric concentrations up to 10% [17]. Early research found that even a small concentration of nanoparticles, 4%, can increase the thermal conductivity of the base fluid by 20% [20]. However, as the volumetric concentration of nanoparticles increases the viscosity of the nanofluid increases substantially [21].

Theoretical and experimental research has attempted to define the thermal properties of nanofluids. Choi [22] used the Dittus and Boelter [23] equation (1.1) to show that the thermal conductivity of a nanofluid is greater than the base fluid.

$$Nu=0.023Re^{0.8}Pr^{0.4} \tag{1.1}$$

Pak and Cho [21] conducted physical experiment with Al_2O_3 and TiO_2 in water at very low concentrations, up to 3%. Their Nusselt number correlation follows the format Dittus-Boelter equation but has different multiplier and Prandtl number power:

$$Nu=0.021Re^{0.8}Pr^{0.5} \tag{1.2}$$

In cold climates fluids with a lower freeze point are added to water to protect infrastructure from freezing. Ethylene and propylene glycol are common freeze protection chemicals that are added to water. These fluids can have up to 60% glycol depending on the low temperature they might encounter. Higher concentrations of glycol raise the viscosity of the fluid and lower the thermal conductivity. Adding nanoparticles to a water/glycol mixture increases the viscosity and the thermal conductivity of the mixture [17]. Eastman et al. found that adding 3% Cu nanoparticles to ethylene glycol increased the thermal conductivity over the base fluid by 40% [24].

Many researchers have evaluated the density property of nanofluids and most have found that the theoretical equation (Equation (1.3)) developed by Pak and Cho [21] compares well with experimental values for a wide variety of nanofluid combinations [17]. Satti et al. [25] found that the Pak-Cho equation was within 4% of several nanofluids based in 60:40 Ethylene glycol/water (EG/W) between 0 and 90°C.

$$\rho_{nf} = \rho_p \emptyset + \rho_{bf}(1 - \emptyset)$$ (1.3)

The viscosity of nanofluids is more dependent on the type nanoparticle and the particular base fluid than the density. Namburu et al. [18] and Sahoo et al. [19] developed correlations for CuO, SiO_2 and Al_2O_3 and 60:40 EG/W nanofluids from physical tests. Sahoo developed a correlation for Al_2O_3 in EG/W down to -35°C. Each correlation was specific to each nanofluid combination. Vajjha and Das [26] used the work of Sahoo et al. and Namburu et al. to develop a viscosity correlation for all three nanofluid combinations (Equation (1.4)).

$$\frac{\mu_{nf}}{\mu_{bf}} = A_1 e^{A_2 \emptyset}$$ (1.4)

A_1 and A_2 are constants based on particle type, size, and concentration from Table 1.1.

Table 1.1. Constants for viscosity correlation from [26].

Nanoparticle	A_1	A_2	Average Particle Size (nm)	Concentration (%)
CuO	0.983	12.959	45	$\emptyset < 0.1$
Al_2O_3	0.9197	22.8539	29	$\emptyset < 0.06$
SiO_2	1.092	5.954	20	$\emptyset < 0.1$
SiO_2	0.9693	7.074	50	$\emptyset < 0.06$
SiO_2	1.005	4.669	100	$\emptyset < 0.06$

Pak and Cho [21] presented an equation for nanofluid specific heat which was from literature for microfluids. Xuan and Roetzel [27] presented an improved correlation assuming thermal equilibrium between the nanoparticles and the base fluid (Equation (1.5)).

$$c_{pnf} = \frac{\emptyset \rho_p c_{pp} + (1 - \emptyset) \rho_{bf} c_{pbf}}{\rho_{nf}}$$ (1.5)

Equation (1.5) is theoretical. Vajjha and Das [17] compared equation 1.5 to measured data for three different nanofluids and found that equation (1.5) compared well.

The thermal conductivity of nanofluids is widely studied [17]. Lee et al. [20] conducted physical measurements of thermal conductivity of Al_2O_3 and CuO in water at concentrations up

to 4%. They determined that the Hamilton-Crosser model of thermal conductivity for two phase solutions with microparticles [28] was not adequate for nanofluids. Das et al. [29] also conducted physical experiments on CuO and Al_2O_3 in water and found that the Hamilton-Crosser equation under predicted the thermal conductivity. Koo and Kleinstreuer [30] developed a laminar flow model for thermal conductivity that uses the Hamilton-Crosser equation but adds the effects of Brownian motion (Equation (1.6)).

$$k_{nf} = \frac{k_p + 2k_{bf} - 2(k_{bf} - k_p)\emptyset}{k_p + 2k_{bf} + (k_{bf} - k_p)\emptyset} k_{bf} + 5 * 10^4 \left(\beta \emptyset \rho_{bf} c_{pbf} \sqrt{\frac{KT}{\rho_p d_p}} \right) f(T, \emptyset) \qquad (1.6)$$

$$f(T, \emptyset) = (-6.04\emptyset + 0.4705)T + (1722.3\emptyset - 134.63)$$

$$\beta = 0.0017(100\emptyset)^{0.0841} \ for\ Al_2O_3$$

$$\beta = 0.0011(100\emptyset)^{-0.7272} \ for\ CuO$$

Vajjha and Das [31] developed correlations for $f(T, \emptyset)$ and β in equation (1.6) for CuO, ZnO, SiO_2, and Al_2O_3 in 60:40 EG/W base fluid (Equation (1.7) and Table 1.2).

$$f(T, \emptyset) = (2.8217 * 10^{-2}\emptyset + 3.917 * 10^{-3}) \left(\frac{T}{T_o} \right) + (-3.0669 * 10^{-2}\emptyset - 3.91123 * 10^{-3}) \qquad (1.7)$$

Table 1.2. Beta correlations for equation 60:40 EG/W [17].

Nanoparticle	β	Concentration	Average Particle Size (nm)	Temperature (K)
CuO	$9.881(100\emptyset)^{-0.9446}$	$\emptyset < 0.1$	29	$298 \le T \le 363$
Al_2O_3	$8.4407(100\emptyset)^{-1.07304}$	$\emptyset < 0.1$	53	$298 \le T \le 363$
SiO_2	$1.9526(100\emptyset)^{-1.07304}$	$\emptyset < 0.1$	30	$298 \le T \le 363$
ZnO	$8.4407(100\emptyset)^{-1.4594}$	$\emptyset < 0.1$	29 & 77	$298 \le T \le 363$

Because the heat pump in this study uses a 20:80 methanol/water mixture, a brief literature review was conducted into methanol based nanofluids. A few [32]–[37] studies have looked at nanofluids with pure methanol base fluids. These are mostly for cooling applications, including methanol heat pipes for cooling electronics. Methanol-based nanofluids improve the thermal conductivity of the fluid over the base fluid 23 to 29% [37]. These studies also found that methanol based nanofluids behave as non-Newtonian fluids [34], [35]. Since 20:80 methanol/water is more water than pure methanol the water based nanofluid correlations will be used in the project.

1.4 Objectives of this Thesis and Summary of Chapters

The objectives of this thesis are to analyze the experimental data of the GSHP at CCHRC and then perform theoretical analysis by considering CuO and Al_2O_3 nanofluids in the GHE of the GHSP.

This study is presented in the following four chapters.

Chapter 2 will present information on the CCHRC GSHP system design, set up and installation. Additionally, analysis of data from the first four heating seasons is presented. A short section of Chapter 2 will look at the heat pump system data in years 5 and 6 which will highlight some of the challenges of in-situ data collection.

Chapter 3 presents a theoretical analysis of adding nanoparticles to the fluid in the GHE in order to improve heat transfer and potentially performance of the heat pump system.

In chapter 4, data from the heat pump system has been used to inform finite element models of the system's interaction with the soil. Two models were developed using Comsol Multiphysics. Those results were presented in Garber-Slaght, et al. [1] and Garber-Slaght, et al. [38]. Those two models are compared to a Temp/W model created for this thesis.

Chapter 5 summarizes the research to date and provides suggestions for future research.

1.5 Nomenclature

GSHP   Ground Source Heat Pump

CCHRC   Cold Climate Housing Research Center

GHE   Ground Heat Exchanger

ACEP   Alaska Center for Energy and Power

EG/W   60:40 Ethylene Glycol and Water

Nu   Nusselt number ($\frac{hD}{k}$)

Re   Reynolds number ($\frac{\rho VD}{\mu}$)

Pr   Prandtl number ($\frac{c_p \mu}{k}$)

c_p Specific heat (J/kg·K)

k Thermal conductivity (W/m·K)

h Convective heat transfer coefficient (W/m^2·K)

K The Stephan Boltzmann constant (1.381 x 10^{-23} J/K)

d Diameter (m)

T Temperature (K)

T_o Reference temperature (273 K)

1.6 Greek Symbols

μ Dynamic Viscosity (mPa·s)

ρ Density (kg/m^3)

$\varnothing$ Volumetric concentration

1.7 Subscripts

nf nanofluid

p particle

bf base fluid

1.8 References

[1] R. Garber-Slaght, R. Daanen, and A. Roe, "Ground source heat pump efficiency in cold climates," *ASHRAE Trans.*, vol. 120, no. 2, 2014.

[2] R. Garber-Slaght and R. Peterson, "Can ground source heat pumps perform well in Alaska?," in *Proceedings of the IGSHPA Technical/Research Conference and Expo 2017*, 2017.

[3] R. Garber-Slaght and J. D. Spitler, "Design of horizontal ground heat exchangers in sub-Arctic conditions—sensitivity to undisturbed ground temperatures," in *Cold Climate HVAC Conference 2018*, 2018, pp. 393–403.

[4] J. Meyer, D. Pride, J. O'Toole, C. Craven, and V. Spencer, "Ground-source heat pumps in cold climates," Denali Commission, Fairbanks, AK, 2011.

[5] W. Wu, B. Wang, T. You, W. Shi, and X. Li, "A potential solution for thermal imbalance of ground source heat pump systems in cold regions: ground source absorption heat pump," *Renew. Energy*, vol. 59, pp. 39–48, 2013.

[6] T. You, W. Wu, W. Shi, B. Wang, and X. Li, "An overview of the problems and solutions of soil thermal imbalance of ground-coupled heat pumps in cold regions," *Appl. Energy*, vol. 177, pp. 515–536, 2016.

[7] P. Eslami-nejad and M. Bernier, "Freezing of geothermal borehole surroundings: A numerical and experimental assessment with applications," *Appl. Energy*, vol. 98, pp. 333–345, 2012.

[8] W. Yang, L. Kong, and Y. Chen, "Numerical evaluation on the effects of soil freezing on underground temperature variations of soil around ground heat exchangers," *Appl. Therm. Eng.*, vol. 75, pp. 259–269, 2015.

[9] G. P. Vasil'ev, V. A. Lichman, N. V. Peskov, and N. L. Semendyaeva, "Modeling the heat regime of thermal boreholes with pore moisture freezing/melting," *Comput. Math. Model.*, vol. 26, no. 3, pp. 336–345, 2015.

[10] A. Rezaei, E. M. Kolahdouz, G. F. Dargush, and A. S. Weber, "Ground source heat pump pipe performance with tire derived aggregate," *Int. J. Heat Mass Transf.*, vol. 55, no. 11–12, pp. 2844–2853, 2012.

[11] Z. Zhihua, Y. Guoqiang, and Z. Xinmiao, "Temperature change of underground in the long running of vertical ground-coupled heat pump," in *2011 International Conference on Electric Technology and Civil Engineering*, 2011, pp. 1643–1646.

[12] K. Bakirci, "Evaluation of the performance of a ground-source heat-pump system with series GHE (ground heat exchanger) in the cold climate region," *Energy*, vol. 35, pp. 3088–3096, 2010.

[13] H. Nielson and J. Zarling, "Ground source heat pump demonstration," Alaska Energy Center, AEC 81-005-1, Fairbanks, AK, 1983.

[14] G. Mueller and J. Zarling, "Ground source heat pump monitoring," Matanuska Electric Association, Inc., 1996.

[15] B. Instantes and A. Instantes, "Foundation design using a heat pump cooling system," in *Ninth International Conference on Permafrost*, 2008.

[16] T. McFadden, "Supplemental research report on foundation stabilization using a heat pump cooling system at 728 Constitution Drive, Fairbanks, Alaska, USA," Permafrost Technology Foundation, Fairbanks, AK, 2007.

[17] R. S. Vajjha and D. K. Das, "A review and analysis on influence of temperature and concentration of nanofluids on thermophysical properties, heat transfer and pumping power," *Int. J. Heat Mass Transf.*, vol. 55, no. 15–16, pp. 4063–4078, 2012.

[18] P. K. Namburu, D. P. Kulkarni, A. Dandekar, and D. Das, "Experimental investigation of viscosity and specific heat of silicon dioxide nanofluids," *Micro Nano Lett.*, vol. 2, no. 3, pp. 67–71, 2007.

[19] B. C. Sahoo, R. S. Vajjha, R. Ganguli, G. A. Chukwu, and D. K. Das, "Determination of rheological behavior of aluminum oxide nanofluid and development of new viscostiy correlations," *Pet. Sci. Technol.*, vol. 27, no. 15, pp. 1757–1770, 2009.

[20] S. Lee, S. U. S. Choi, S. Li, and J. A. Eastman, "Measuring thermal conductivity of fluids containing oxide nanoparticles," *J. Heat Transfer*, vol. 121, pp. 280–289, 1999.

[21] B. C. Pak and Y. I. Cho, "Hydrodynamic and heat transfer study of dispersed fluids with submicron metallic oxide particles," *Exp. Heat Transf.*, vol. 11, no. 2, pp. 151–170, 1998.

[22] S. U. S. Choi, "Enhancing thermal conductivity of fluids with nanoparticles," in *Developments and Applications of Non-Newtonian Flows*, D. A. Siginer and H. P. Wang, Eds. New York: ASME, 1995, pp. 99–105.

[23] F. W. Dittus and L. M. . Boelter, "Heat Transfer of automobile radiators of the tubular type," *Publ. Enigneering*, vol. 2, no. 443, 1930.

[24] J. A. Eastman, S. U. S. Choi, S. Li, W. Yu, and L. J. Thompson, "Anomalously increased effective thermal conductivities of ethylene glycol-based nanofluids containing copper nanoparticles," *Appl. Phys. Lett.*, vol. 78, no. 6, pp. 718–720, 2001.

[25] J. R. Satti, D. K. Das, and D. R. Ray, "Measurements of Densities of Propylene Glycol-Based Nanofluids and Comparison With Theory," *J. Therm. Sci. Eng. Appl.*, vol. 8, no. 2, p. 021021, 2016.

[26] R. S. Vajjha and D. K. Das, *Measurements of thermophysical properties of nanofuids and computation of heat transfer characteristics*. Lambert Academic Publishing, 2010.

[27] Y. Xuan and W. Roetzel, "Conceptions for heat transfer correlation of nanofluid," *Int. J. Heat Mass Transf.*, vol. 43, pp. 3701–3707, 2000.

[28] R. L. Hamilton and O. K. Crosser, "Thermal conductivity of hetrogeneous two-component

systems," *Ind. Eng. Chem. Fundam.*, vol. 1, pp. 187–191, 1962.

[29] S. K. Das, N. Putra, P. Thiesen, and W. Roetzel, "Temperature dependence of thermal conductivy enhancement for nanofluids," *J. Heat Transfer*, vol. 125, pp. 151–155, 2003.

[30] J. Koo and C. Kleinstreuer, "Laminar nanofluid flow in microheat-sinks," *Heat Mass Transf.*, vol. 48, pp. 2652–2611, 2005.

[31] R. S. Vajjha and D. K. Das, "Measurement of thermal conductivity of three nanofluids and development of new correlations," *Int. J. Heat Mass Transf.*, vol. 52, pp. 4675–4682, 2009.

[32] C. Pang, J.Y. Jung, and Y. T. Kang, "Thermal conductivity enhancement of Al_2O_3 nanofluids based on the mixtures of aqueous NaCl solution and CH_3OH," *Int. J. Heat Mass Transf.*, vol. 56, no. 1–2, pp. 94–100, Jan. 2013.

[33] C. Pang, J.Y. Jung, J. W. Lee, and Y. T. Kang, "Thermal conductivity measurement of methanol-based nanofluids with Al_2O_3 and SiO_2 nanoparticles," *Int. J. Heat Mass Transf.*, vol. 55, no. 21–22, pp. 5597–5602, 2012.

[34] R. M. Mostafizur, A. R. Abdul Aziz, R. Saidur, and M. H. U. Bhuiyan, "Investigation on stability and viscosity of SiO_2-CH_3OH (methanol) nanofluids," *Int. Commun. Heat Mass Transf.*, vol. 72, pp. 16–22, 2016.

[35] R. M. Mostafizur, A. R. Abdul Aziz, R. Saidur, M. H. U. Bhuiyan, and I. M. Mahbubul, "Effect of temperature and volume fraction on rheology of methanol based nanofluids," *Int. J. Heat Mass Transf.*, vol. 77, pp. 765–769, Oct. 2014.

[36] R. M. Mostafizur, R. Saidur, A. R. Abdul Aziz, and M. H. U. Bhuiyan, "Thermophysical properties of methanol based Al_2O_3 nanofluids," *Int. J. Heat Mass Transf.*, vol. 85, pp. 414–419, 2015.

[37] R. M. Mostafizur, M. H. U. Bhuiyan, R. Saidur, and A. R. Abdul Aziz, "Thermal conductivity variation for methanol based nanofluids," *Int. J. Heat Mass Transf.*, vol. 76, pp. 350–356, Sep. 2014.

[38] R. Garber-Slaght, C. Craven, R. Peterson, and R. Daanen, "Ground source heat pump demonstration in Fairbanks , Alaska," Cold Climate Housing Research Center, Fairbanks, AK, 2017.

Chapter 2: The CCHRC Heat Pump Demonstration Project

2.1 Introduction

Ground source heat pumps (GSHPs) are often a more cost effective space conditioning systems than traditional air conditioner and boiler/furnace systems. They are more effective because they extract (or deposit) a portion of the energy they provide from the soil. In a heating application, the warmer the soil the more efficient the heat pump. There are few long term studies of GSHPs in a heating dominated climate where the soil temperature is low, around 0°C [1].

The GSHP demonstration project at the Cold Climate Housing Research Center (CCHRC) was designed to install and to evaluate the performance of a GSHP in a cold climate for at least 10 years. These are the project objectives:

1. Determine if long-term performance of a GSHP is stable in a severe cold climate, and thoroughly characterize its efficiency over multiple heating seasons.
2. Evaluate if thermal degradation of the ground loop field is a fundamental challenge for adoption of the technology in cold climates.
3. Examine the significance of practical and affordable ground surface treatments to maximize energy capture in the ground.
4. Compare the primary energy consumption and greenhouse gas emissions of the GSHP installation relative to conventional heating systems [2].
5. Demonstrate the viability of a GSHP at its most northern (coldest) limit of operation.

The system was installed in 2013 and only runs in heating mode. It has been operating for 6 years, however, this thesis only evaluates the first 4 years.

2.2 Background

CCHRC's Research and Testing Facility (RTF) is located on the campus of the University of Alaska Fairbanks (UAF) (Figure 2.1). Fairbanks has 7,509°C heating degree-days$_{18}$ and 40°C cooling degree-days$_{18}$ the 99.6% design temperature is -41.9°C [3]. Fairbanks is in a zone of discontinuous and warm permafrost (0°C). The area surrounding the RTF is an open field cleared of native vegetation more than 60 years ago and is made up of moist silt [4]. The permafrost in the area underlying and around the RTF has been degrading since the land was first cleared [4].

The RTF is 2,044 m^2 with 3 distinct heating sections. The heat pump was sized to heat the

464 m^2 office space on the east side of the building with a design heat load of 17.6 KW. Heat is distributed to the area via an in-floor hydronic tubing system embedded in concrete. The office space has 9 thermostatically controlled zone valves. The heat pump system replaced a 22.3 KW oil fired condensing boiler as the main source of heat for this portion of the building; a masonry stove is still used for supplemental space heating.

Figure 2.1. CCHRC's Research and Testing Facility. The original building (the right side of the photo) was built in 2006; the addition on the left was completed in 2012. The heat pump heats the section on the far right end of the photo.

2.2.1 Design and Installation

The soils around the RTF have been extensively surveyed in the past 20 years for road and building construction projects. Borehole logs from these surveys were used to inform the design of the heat pump ground heat exchanger (GHE). Boreholes drilled on the site in 2006 prior to the construction of the RTF found the site underlain with a sloping layer of permafrost. The top of the layer started at 3 m on the south side of the building near the undisturbed vegetation and sloped down to 9.1 m on the north side where the native vegetation had been cleared. Data collected under the east end of the RTF since 2006 shows that the permafrost table has further degraded by an additional 0.6 m. A test borehole northwest of the RTF in 2012, prior to

installing the GHE, did not find permafrost within 9.1 m of the surface. All the soils were found to be moist silt.

A soil thermal conductivity (TC) test was conducted in October 2012, one year prior to the installation of the heat pump. A 34 m long horizontal loop at 2.7 m of depth was installed 12 days prior to the testing. The test lasted 48 hours. A 20:80 methanol/water solution was run through the piping. Energy was added to the fluid via an electric heating coil. The temperature change in fluid and the energy input into the system was recorded. Geothermal Resource Technologies, Inc. evaluated the data and determined the soil thermal conductivity was 1.42 W/m·K. The thermal diffusivity was estimated to be 0.055 m^2/day.

CCHRC originally wanted to demonstrate both deep wells and horizontally trenched GHEs. However, test bores for Thompson Drive (about 180 m away from the GHE) construction in 2001 discovered frozen schist bedrock from 19.5 m down to 45.7 m (the bottom of the boreholes)[4]. The frozen schist was -0.2 °C. The large layer of frozen bedrock was deemed to be too poor a conductor of energy for this demonstration. A horizontal GHE was designed based on the technology available in Fairbanks at the time. Since directional drilling was not an option, horizontal "slinky" coils were developed. Six 30.5 m long by 1 m wide slinky coils with an 0.5 m pitch were installed 1.8 m apart (see Figure 2.2). Overall, 1,463 lineal m of 1.9 cm HDPE was installed at 2.7 m depth to create the in-ground heat exchanger. The GHE size and depth were determined by knowledge of past installations in the area, in conjunction with ground thermal conductivity test data, and information from a finite element model. Additionally, IGSHPA (International Ground Source Heat Pump Association) guidelines for flow path (one 30 m slinky coil per ton of capacity) and turbulent flow were used to further guide the design of the ground heat exchanger [5].

The depth of the GHE is more than was recommended by the Mueller and Zarling [6] and Nielsen and Zarling's [7] Alaskan studies. However, the depth was chosen to be below the line of seasonal frost (about 1.2 m) and above the top of the permafrost (near 9.1 m). In addition, the 2.7 m depth is the typical installation depth for residential horizontal GHE in the Fairbanks area. One of the initial topics of this project was to determine the optimal depth of the GHE [2]. The 2017 model found that the optimal depth for these design conditions is around 2.5 m.

This study also evaluates the effects of different ground coverings and which are more advantageous for energy recharge. Three different coverings are being evaluated: dark rocks,

sand, and grass. Each treatment covers 2 slinky loops (see Figure 2.2). The soil temperatures under the coverings are monitored as are the temperatures of the fluid returning from the slinky coils.
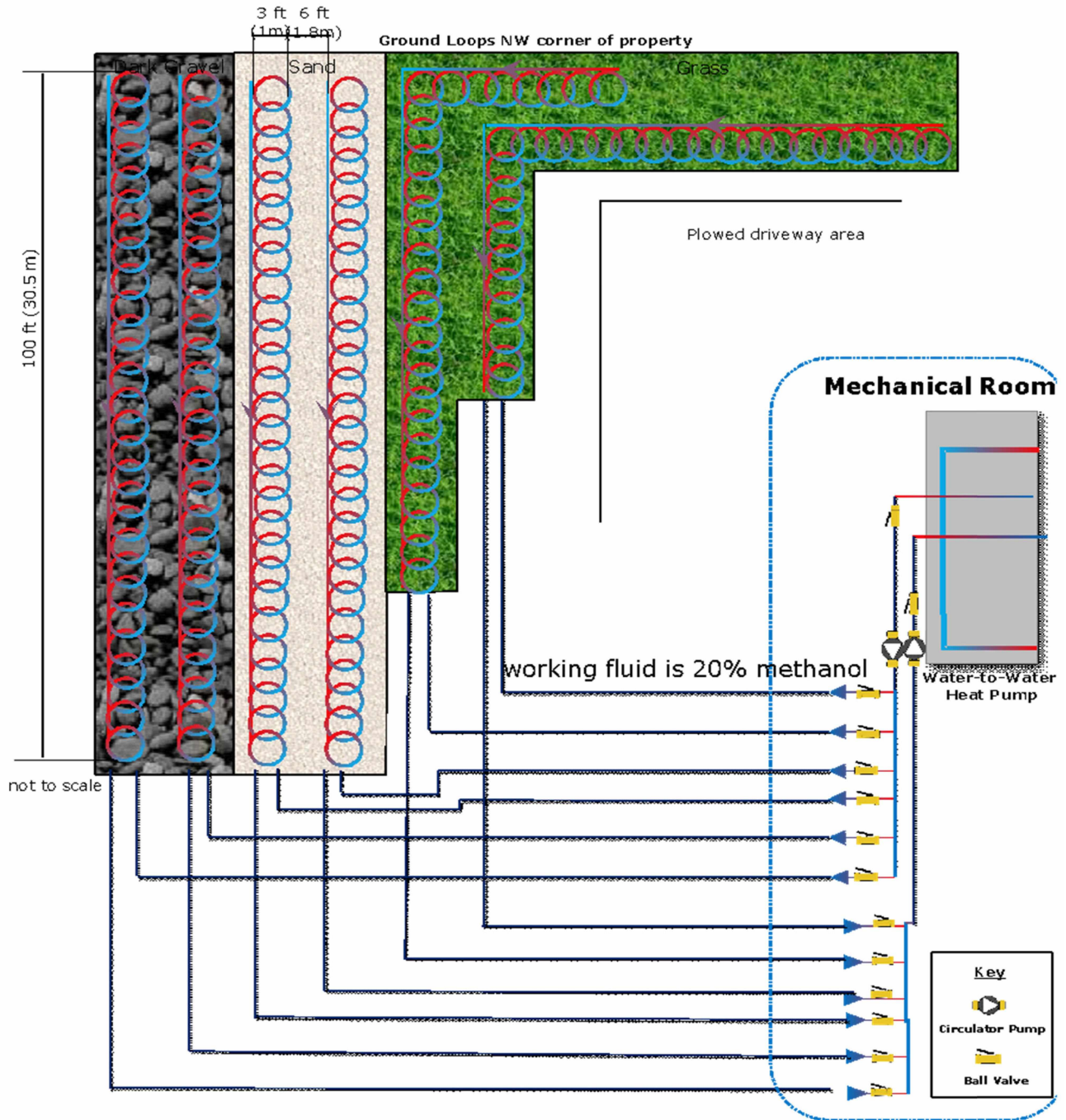
Figure 2.2. Schematic of the heat pump layout. The GHE is to the northwest of the RTF. (The schematic is not to scale.)

2.2.2 The Heat Pump Unit

The heat pump is a residential 21 kW water-to-water unit, selected based on previous experience with the model in Fairbanks. The unit is a GeoSource Hydronic RGS-W072 with a single stage compressor. It is rated to have a COP of 3.4 at 0°C entering water temperature and 68 l/min of flow from the GHE and flow to the buffer tank. The GHE installed flow is 63 l/min and the flow to the buffer tank is 65 l/min.

The heat pump heats a 303 liter buffer tank of water to a temperature determined by the outdoor set point curve. The minimum temperature set point for the buffer tank is 26.7°C and the maximum is 42.8° C. Originally, the set point curve had a maximum of 41.7°C ; however the in-floor heating tubes are configured in a way that requires a higher temperature so the set point curve was changed. This higher set point lowers the efficiency of the heat pump slightly. The GHE side of the heat pump is charged with a 20% methanol/80% water mixture. The building hydronic side of the heat pump is charged with water.

2.2.3 Maintenance and History

The heat pump was installed between May 2013 and October 2013. The GHE was installed in May to take advantage of the stability of the frozen ground (Figure 2.3). Six 2.7 m deep trenches were dug, while the first 0.6 to 1.2m of soil was frozen making certain that the soils did not slump into the trenches. In October 2013 the plumbing for the heat pump was completed (Figure 2.4) and the unit was started and commissioned. The data collection system came online in November 2013.

The heat pump itself has had two warranty callbacks, both related to faulty electrical parts. In November 2013 a contact and the control board were replaced, and in February 2016 a contactor was replaced. The GHE and the circulation pumps have not required any maintenance.

In October 2018 the heat pump thermostatically controlled valve (TXV) failed. This failure was outside of the warranty period and cost $1,074 to repair. Data from this failure is not presented in this thesis but will be studied in future research.

Figure 2.3. GHE slinky coil installation. The installation of the GHE required a large excavation that took nine days.

Figure 2.4. Heat pump and plumbing installation. The heat pump plumbing involved setting the heat pump and the buffer tanks and connecting all the parts with copper pipe.

2.3 Data Collection

The automated data collection system is composed of several components listed in Table 2.1 and shown in Figure 2.5 on the system diagram.

Table 2.1. Data Collection System Components.

Data Point	Sensors and Location	Range and Accuracy
Ground Temperatures	Thermistors within and around the GHE	-20°C to 80°C ±0.1°C
Manifold	Thermistors in the manifold returning from	-20°C to 80°C ±0.1°C
Ground Loop Energy	BTU meters in the piping to and from the GHE	0 to 75.6 l/min ±2%
Heat Pump Energy	In the piping to and from the buffer tank and	0 to 56.8 l/min ±2%
Heat Pump Electrical	Heat pump and the circulating pumps	0 to 100 amp ±1%
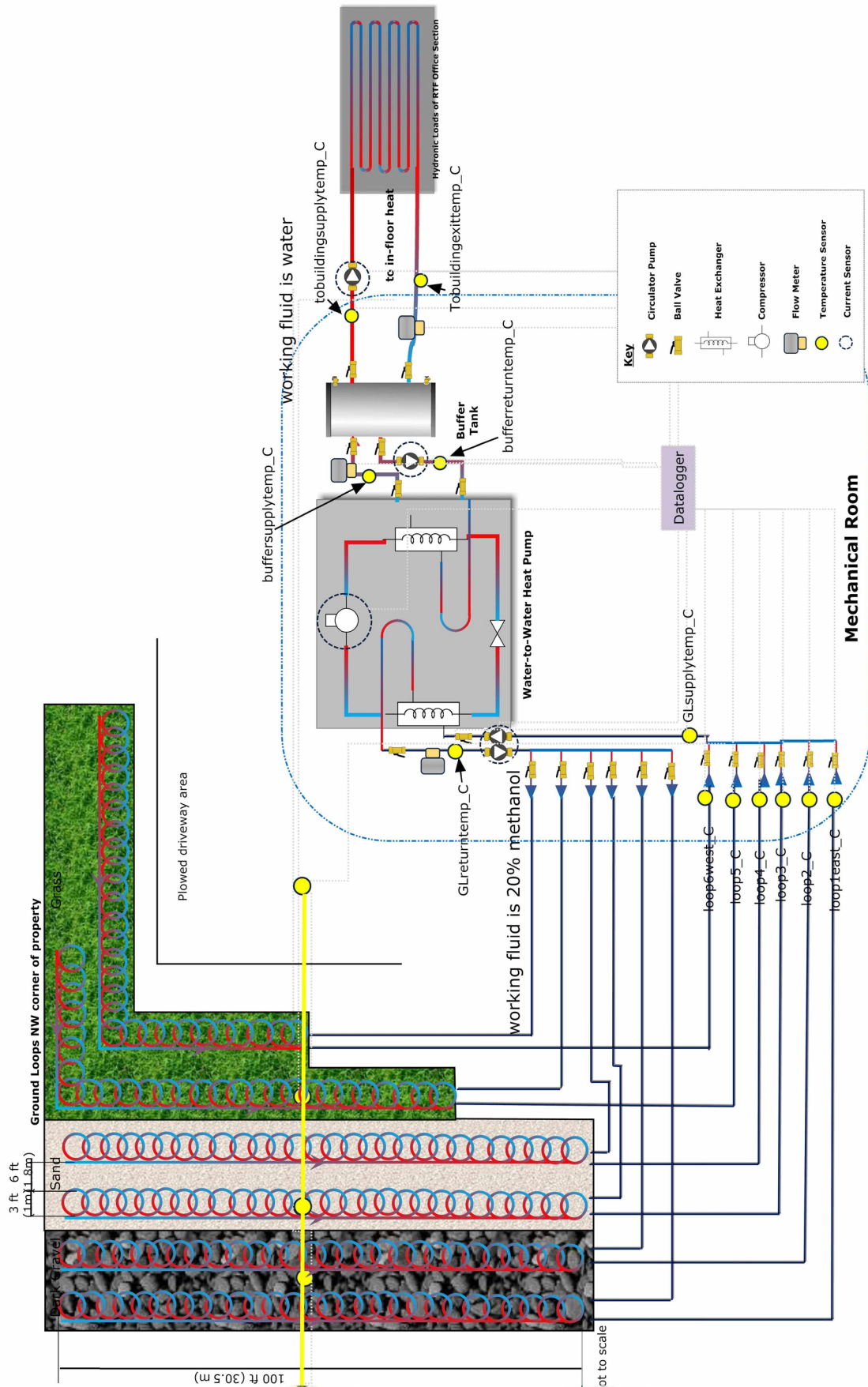
Figure 2.5. Data collection system. Each temperature data point in the GHE has multiple temperature sensors going to depth under it. (The schematic is not to scale.)

18

2.3.1 Ground Heat Exchanger

Temperatures and soil freezing front data is being collected in the GHE. The automatic data collection system is collecting temperature data from 7 temperature strings in and around the GHE (Figure 2.6) as well as the temperatures of the fluid entering the building at the manifold from each heat extraction slinky coil.
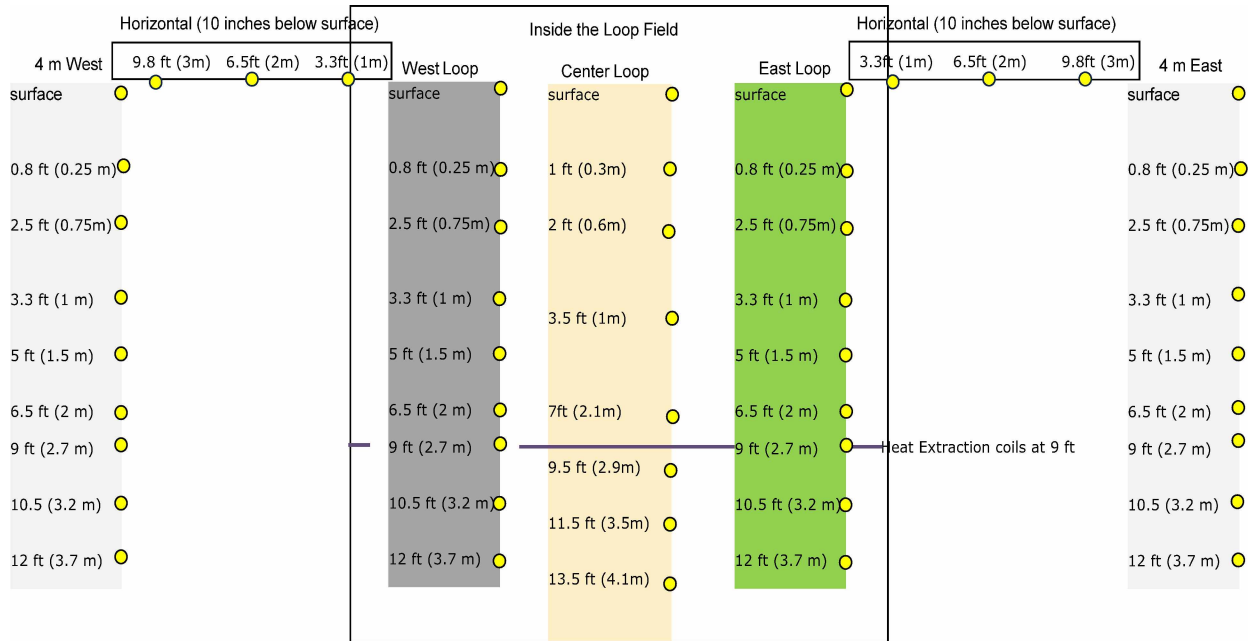
Figure 2.6. In-ground temperature strings. Some of the sensors in this configuration have failed in four years. Some have been replaced but most are not accessible.

The GHE temperatures are used to determine if the ground heat extraction coils are cooling the soil more than the solar recharge in the summer can recover. The temperatures are taken across the surface of the loop field, as shown by the yellow line across the loop field in Figure 2.5. They are also taken down into the GHE field, as far down as 4.1 m in the center of the GHE field. Two of the vertical temperature strings are located in the middle of the slinky coils, while the third is between two sets of coils. The ground heat extraction coils cross the vertical temperature strings at approximately 2.7 m from the surface. Two other vertical temperature strings are 4 m to the west and east sides of the GHE field.

The sensors in the manifold record the temperature of the fluid as it comes back from the GHE field (Figure 2.7). These temperatures were intended to verify whether or not the surface treatments were creating any differences in temperature in each slinky coil loop.

Figure 2.7. GSHP manifold. The manifold is located in the mechanical room. Temperature sensors are in thermowells on the return loop from the ground side of the GHE (the bottom in this photo).

In addition to recording ground temperatures, permafrost tubes are installed in three locations in and around the GHE. A permafrost tube consists of a thin column of dyed water within a pipe in the ground (Figure 2.8). Once a month the tubes are pulled out of the ground and the depth and extent of the ice within the water column is recorded. There are 2 permafrost tubes within the GHE (one in the center of a sand loop and one between the two gravel loops) and one in the field to the west of the GHE.

Figure 2.8. Checking permafrost tubes. The separated lines of blue in the right hand photo indicate areas of frozen ground.

The temperatures from the GHE are used to chart the change in soil temperature over time at

certain depths. Additionally, the temperatures are used to create whiplash curves for the GHE. Whiplash curves are configured to show the temperature on the x-axis and the depth of the soil on the y-axis. This configuration creates a visual analysis of the changes in ground temperature over time. Since a 0°C temperature in the ground loop does not necessarily indicate frozen soil (it is more an indication that phase changing is occurring), the permafrost tubes are used to verify if the water in the soil is frozen. As energy is extracted from the GHE the temperature drops to 0°C quickly, and once the freezing temperature is reached the energy that is extracted changes the phase of the water in the soil to a solid. This phase change takes much longer than the temperature changes and the soil is not necessarily frozen at the freezing temperature. Locations that stay below the freezing temperature for more than 2 years are then considered permafrost.

2.3.2 Mechanical System

The automated data collection system is also collecting data on the mechanical side of the heat pump. The heat pump uses two circulation pumps to pump fluid through the GHE and an additional one to pump hot water to the buffer tank. The electrical use of the heat pump is monitored as is the electrical use of each pump individually. A fourth circulation pump, which delivers hot water from the buffer tank to the in-floor distribution coils in the building, is also monitored for electrical use.

Three heat energy locations are monitored using flow and temperature sensors: the energy delivered to the heat pump from the GHE, the energy from the heat pump to the buffer tank, and the energy from the buffer tank to the building.

The oil-fired condensing boiler replaced by the heat pump is still on site and can be used as a backup system should the heat pump ever fail. The energy output of the condensing boiler is monitored to verify if the boiler is augmenting the heat pump. The masonry stove is still used to heat the same area as the heat pump. The amount of wood added to the stove is recorded to verify how much the heat pump is offset by the stove.

The efficiency of a heat pump or the Coefficient of Performance (COP) is calculated using Equation (2.1).

$$COP = \frac{Heat\ Energy\ to\ the\ Building}{Electricity\ for\ the\ Heat\ Pump} \tag{2.1}$$

"Electricity for the heat pump" includes the electricity powering the heat pump and the 3 circulation pumps (2 to the GHE and one to the buffer tank) that are controlled by the heat pump.

Data is collected on an hourly basis but the COP is calculated as an average for each month.

2.4 Installation Costs

Prior to the design and installation of the heat pump, CCHRC performed the previously mentioned thermal conductivity (TC) test in the soil near the future GHE. A TC test is not commonly performed for residential GSHP system designs, therefore the added cost for the TC test is not included as part of normal design and heat pump installation costs (TC test costs are listed in Table 2.2.). The TC test was completed to ensure the GSHP system design would be optimized and to provide better input data for the finite element model analysis. CCHRC worked with Geothermal Resources Technologies Inc. (GRTI) and Alaska Geothermal, LLC to conduct a TC test.

Table 2.2. Soil thermal conductivity testing.

Component	Cost
Excavation	$2,875
Equipment Shipping	$632
Equipment Rental	$1,150
Data Analysis	$800
Total	$5,457

The costs for the overall heat pump installation (minus the TC test and the data collection system) are presented in Table 2.3. This installation was more expensive than a typical residential installation due in part to the fact that this is a research project and has some unique features (i.e. manifold inside the building). Residential GSHP installations in the Fairbanks area generally cost between $20,000 and $35,000 in total to install [8].

Table 2.3. Heat pump system installation costs.

Component	Cost
System Design	$1,162
GHE Installation	$30,305
Heat Pump Installation	$22,546
Total	$54,014

2.4.1 Operating Cost

The maintenance costs to operate the heat pump have been minimal. Two previously mentioned electrical problems were solved under warranty. The failure of the TXV in 2018 was outside of the warranty and cost $1,074 to repair.

Over the course of the first four operating years the system used 26,517 kWh of electricity. This amounts to $6,361 in heating costs at a constant $0.24 per kWh. Figure 2.9 shows the electrical cost trends by month.
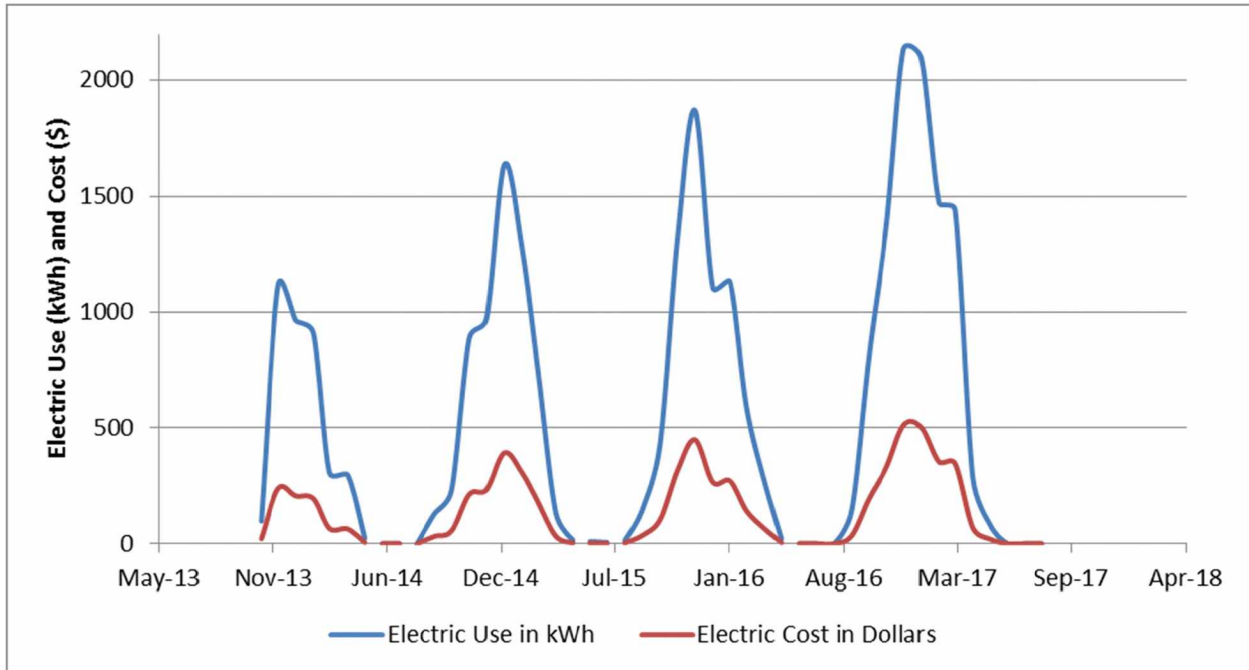
Figure 2.9. Electrical use of the heat pump system. Each successive winter has seen a rise in the electrical use and cost for operating the heat pump.

Table 2.4 breaks out electrical use and cost by month. The heat pump has a small electrical load of 13 W when it is not running. This load runs the thermostat which keeps the buffer tank at a set point based on the outdoor temperature. Each summer, except for 2015, CCHRC turned off the heat pump when the heating season was over in late May and kept it off into September. This off time is indicated by a 0 in the table. The summer of 2015 provides an example of how much the heat pump costs in idle mode, as it was not turned off that summer.

Table 2.4. Annual electrical costs.

	Year 1 (winter 2013-14)		Year 2 (winter 2014-15)		Year 3 (winter 2015-16)		Year 4 (winter 2016-17)	
	Electric Use (kWh)	Electric Cost	Electric Use (kWh)	Electric Cost	Electric Use (kWh)	Electric Cost	Electric Use (kWh)	Electric Cost
August			0	$0.00	13	$3.12	0	$0.00
September			129	$30.96	154	$36.96	146	$35.14
October			229	$54.96	434	$104.16	803	$192.69
November	97	$23.28	885	$212.40	1332	$319.68	1370	$328.81
December	1,115	$267.60	971	$233.04	1871	$449.04	2133	$511.98
January	962	$230.88	1636	$392.64	1104	$264.96	2096	$503.13
February	908	$217.92	1272	$305.28	1129	$270.96	1471	$353.14
March	306	$73.44	740	$177.60	593	$142.32	1442	$346.12
April	297	$71.28	132	$31.68	272	$65.28	286	$68.74
May	24	$5.76	14	$3.36	39	$9.36	83	$19.94
June	0	$0.00	9	$2.16	0	$0.00	0	$0.00
July	0	$0.00	5	$1.20	0	$0.00	0	$0.00
Annual Total	3,709	$890.16	6,022	$1,445.28	6,941	$1,665.84	9,830	$2,359.70

2.5 Savings of the Heat Pump over Using Oil

The amount of savings over using an oil-fired boiler is heavily dependent on the cost of oil per gallon and the efficiency of the oil-fired boiler. Oil prices have been variable since the start of this project; Table 2.5 shows the change in heating fuel costs over the first 4 years of heat pump operation. The cost of electricity has remained consistent at $0.24/kWh over the first 4 years of the project.

Higher oil prices mean more savings when using the heat pump. Table 2.6 shows the savings in using the heat pump over the first 4 years of operation, using the real cost of fuel over that time period. In order to determine an oil-fired BTU equivalent to the amount of heat delivered by the heat pump, a 96% efficient oil-fired condensing boiler was used. This boiler was similar to the one the heat pump replaced; however the high efficiency of this model is not typical of most boilers.

When oil prices slipped below $2.45 per gallon in the third winter, the savings advantage of the heat pump ceased. In fact, using the oil condensing boiler would have saved $207 over using the heat pump in the 2015-16 heating season. In four years the heat pump has saved a combined total of $707 over using the oil fired condensing boiler that is 96% efficient. Replacing an 80%

24

efficient boiler would have increased the savings to $1,676. Had fuel prices remained near $4 per gallon the heat pump system would have saved an estimated $3,421 over the 96% efficient boiler and $4,803 over the 80% efficient boiler in 4 years.

Table 2.5. Heating fuel prices per gallon.

	Year 1 (winter 2013-14)	Year 2 (winter 2014-15)	Year 3 (winter 2015-16)	Year 4 (winter 2016-17)
August		$3.98	$2.97	$2.29
September		$3.72	$2.97	$2.29
October		$3.67	$2.40	$2.31
November	$3.85	$3.67	$2.37	$2.31
December	$3.85	$3.47	$2.35	$2.30
January	$3.92	$3.01	$2.06	$2.40
February	$3.98	$2.76	$1.99	$2.40
March	$3.98	$2.97	$2.02	$2.38
April	$3.98	$2.97	$2.11	$2.43
May	$3.98	$2.97	$2.11	$2.43
June	$3.98	$2.97	$2.11	$2.43
July	$3.98	$2.97	$2.11	$2.43

Table 2.6. Savings of the heat pump system compared to equivalent heating oil use.

	Year 1 (winter 2013-14) Heat Pump savings over oil	Year 2 (winter 2014-15) Heat Pump savings over oil	Year 3 (winter 2015-16) Heat Pump savings over oil	Year 4 (winter 2016-17) Heat Pump savings over oil
August				
September		$27.78	$9.75	($10.93)
October		$113.62	($3.56)	($44.97)
November	$18.12	$146.29	($10.57)	($17.23)
December	$161.28	$135.95	($34.56)	($38.21)
January	$158.10	$93.83	($47.31)	($79.05)
February	$147.28	$42.69	($60.87)	($55.53)
March	$57.70	$53.31	($35.22)	($59.62)
April	$58.42	$21.92	($21.29)	($17.95)
May	$2.65	$3.83	($3.67)	($4.44)
June				
July				
Annual Total	$603.55	$639.22	($207.30)	($327.94)

25

2.6 CCHRC GSHP Results

2.6.1 Observed GHE Temperatures

Temperatures recorded in and around the GHE show cooling of the ground over the four years the heat pump has been in use when compared to the baseline data (Figure 2.10). The temperatures in the vicinity of the heat extraction coils are lower than the baseline temperatures in the adjacent field. The temperature at the depth of the coils shows 0°C most of the winter; the baseline temperatures are 3 to 4°C higher. The temperature around the coils has not dropped below 0°C as the energy of phase change is extracted from the surrounding soils, creating ice in the soil. To date, the soil around the loops has risen above freezing each summer.
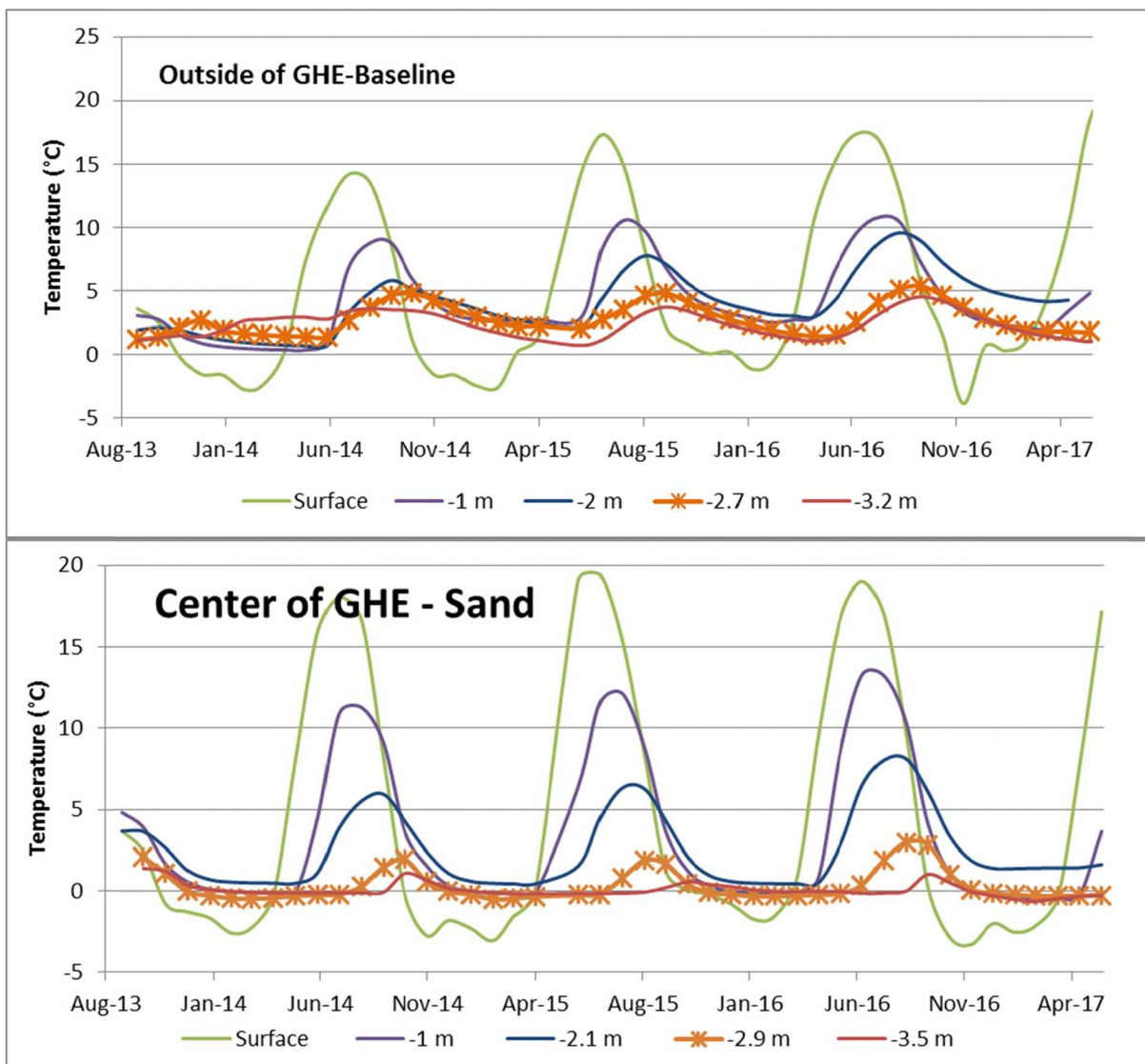
Figure 2.10. In-ground temperatures over time. The starred line is nearest to the ground heat extraction coils. Temperatures are cooler in the GHE than in the field next to the GHE. The surface temperature for the sand was warmer than the field, the field sensors are under grass.

Figure 2.11 shows data into the ground outside the influence of the GHE as a comparison to Figure 2.12, which shows the temperatures into the ground at the center of the GHE over four years. The 2.7 m depth of GHE line in the diagram is where the slinky coils were designed to be, however with a large excavation and backfilling and leveling, it is likely that the coils are not exactly at this level.
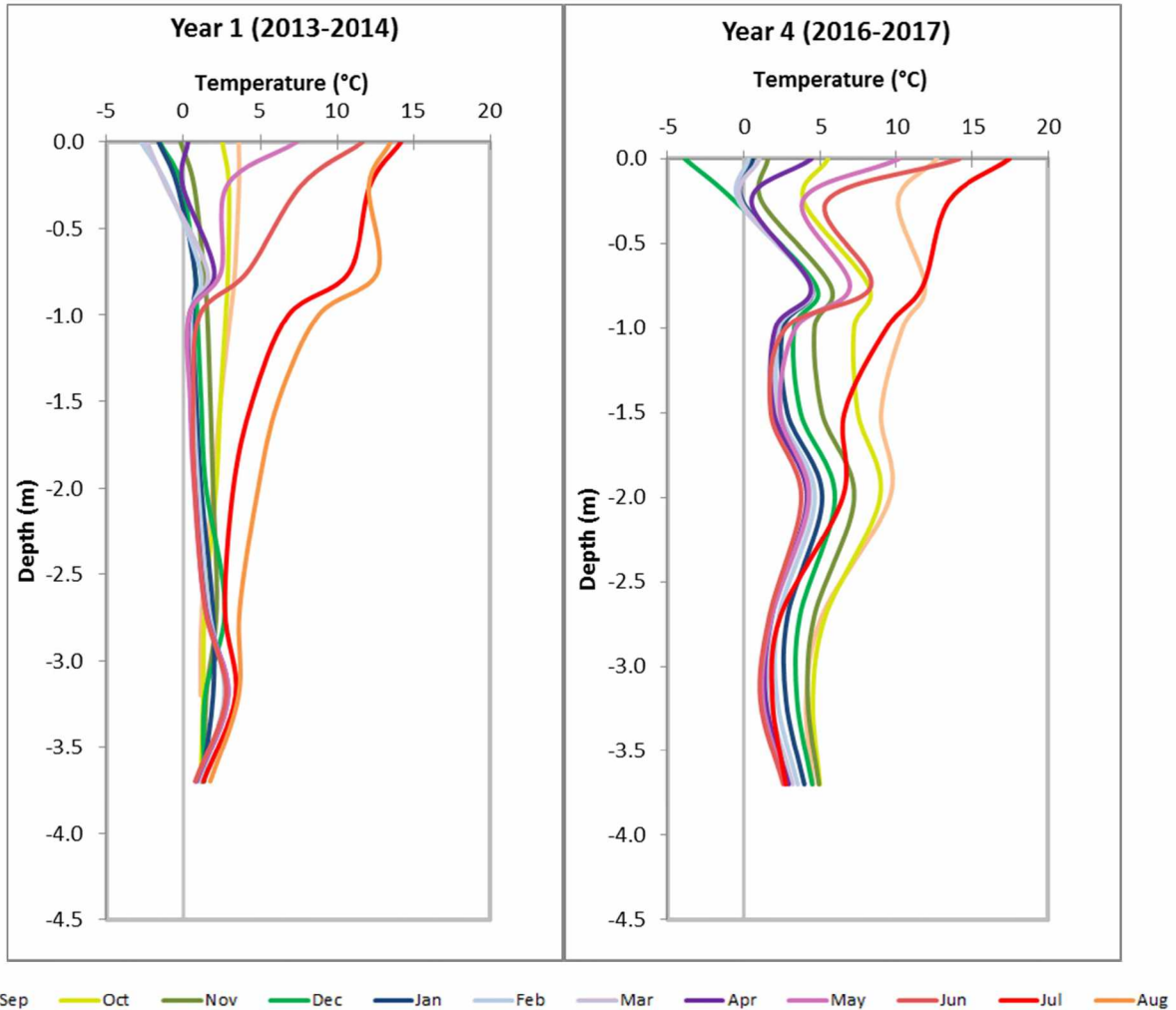
Figure 2.11. Whiplash curve for the baseline data. This is outside of the heat pump field and provides an example of what typical whiplash curve looks like with no influence beyond ambient conditions. The warming of the ground at 3.7 m is potentially the result of rising ground water

Temperatures below the level of the GHE started dropping to freezing the first winter of heat extraction and stayed near freezing throughout the 2015-2016 winter. However, they were above freezing in the fall of 2016 (rising groundwater in this area could be creating warmer conditions, which will be studied in later reports). Overall temperatures have not dropped much below 0°C in four years, but could if permafrost develops around the GHE.
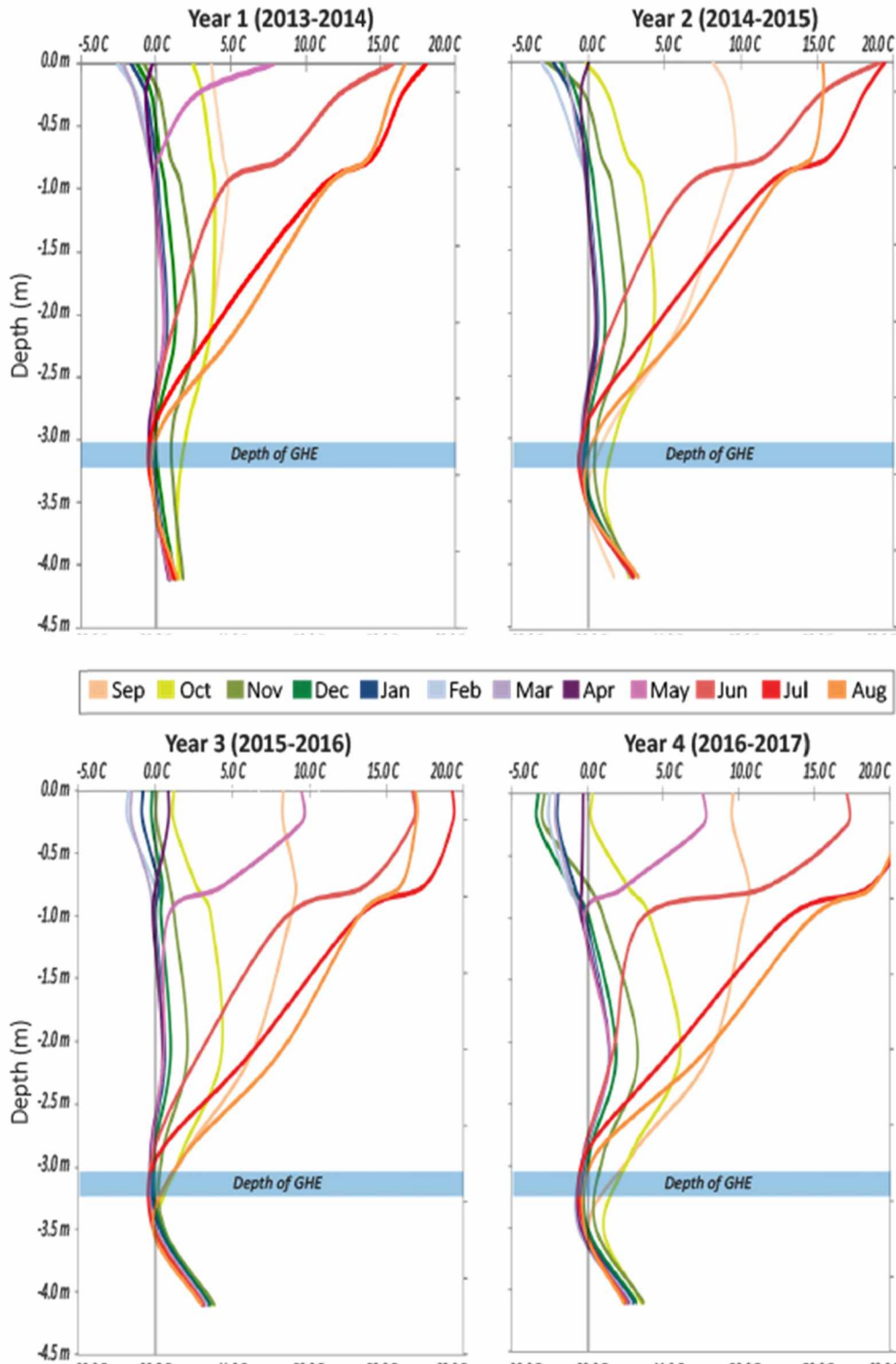
Figure 2.12. Whiplash curves of the center of the GHE (in the sand loop) for four years. Each winter season starts in September and ends in August. The warming at depth agrees with the baseline data and is possibly the result of rising groundwater.

2.6.2 Permafrost

The permafrost tubes in the GHE show some frozen sections of soil within the area of the slinky coil in the center of the GHE. Figure 2.13 shows the extent of frozen ground during the third and fourth winter. To date, the ice around the slinky coils has not lasted the full year. There was no ice below the active layer in any other locations or in any previous year.
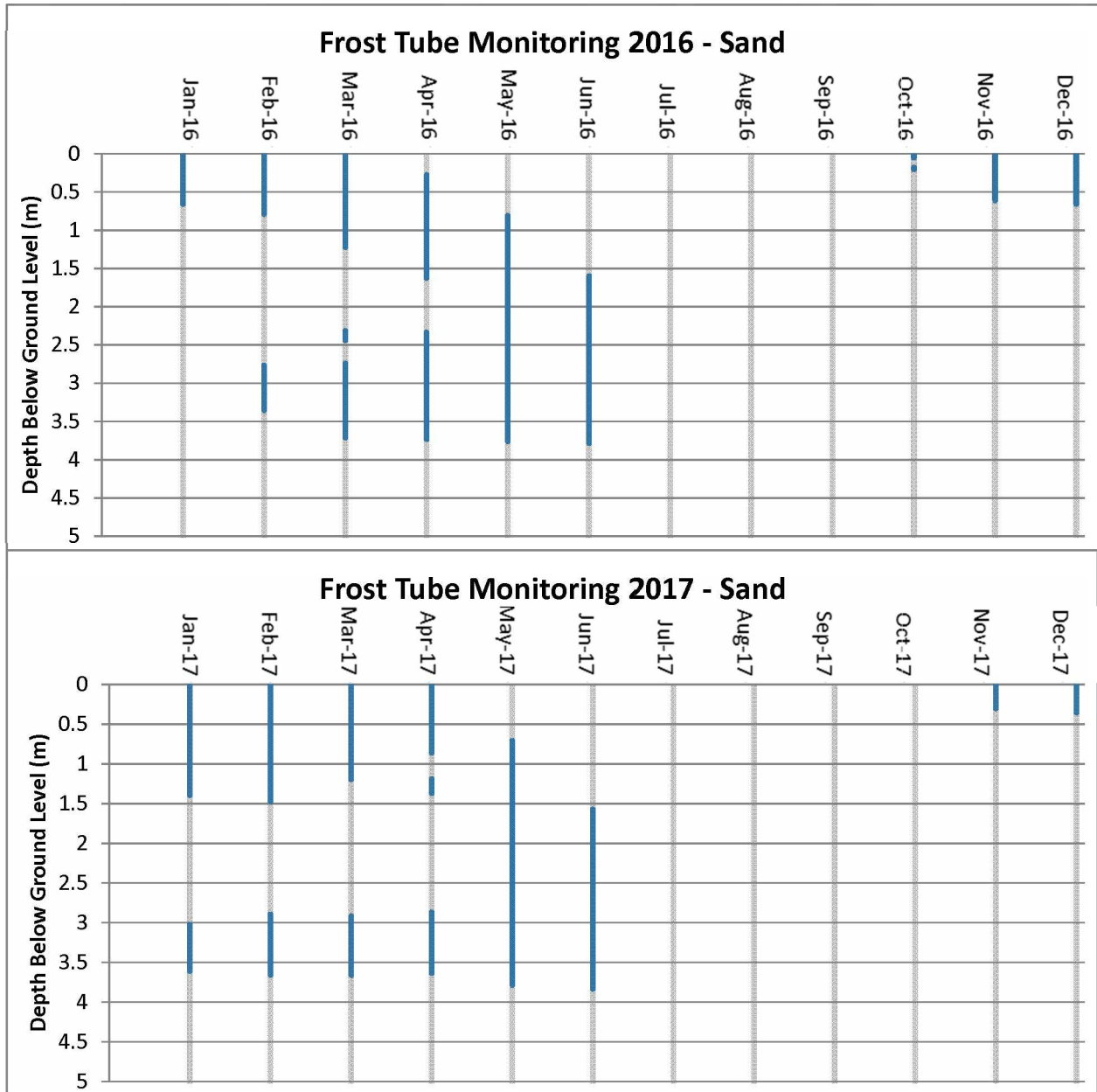
Figure 2.13. Ice in the center of the GHE under the sand treatment. There was no ice in July or August 2016 or 2017. Presently this is the only location that has recorded frozen soil below the active layer.

2.6.3 Surface treatments

Temperatures in the GHE show the effects of the differing surface treatments. Further down in the ground loop the effects of the surface treatments are harder to discern, especially around the slinky coils where the heat extraction has an overwhelming effect on the ground temperatures. However, the dark gravel is keeping that section of the GHE warmer than the sand or the grass. The grass is the coolest of the three treatments. Figure 2.14 shows the temperatures within the GHE over time, based on the surface treatments. Data from all the sensors are not available, but the gravel area temperatures trend higher than the other two treatments over time, with the deeper points having higher temperatures than the deeper points of sand and grass areas.

The temperature sensors in the manifold were set up to determine if the surface treatments were having any effect on the GHE. Figure 2.15 shows the fluid returning from the gravel loops is always slightly warmer than the other two surface treatment loops. The differences in the surface treatments are noticeable in the fall of 2015, with the gravel 0.5°C warmer than the sand loops and 1°C warmer than the grass loops. As winter progressed the gravel loops stayed warmer than the other loops but there was not as much of a difference. The sand loops ended the winter season with the coldest temperatures.

According to the manufacturer's information on this heat pump model, a 0.6C° change in the incoming temperature for the heat pump creates a 0.044 change in the COP of the heat pump. The 1C° increase in the temperatures coming back from the ground loop could improve the COP by 0.08.
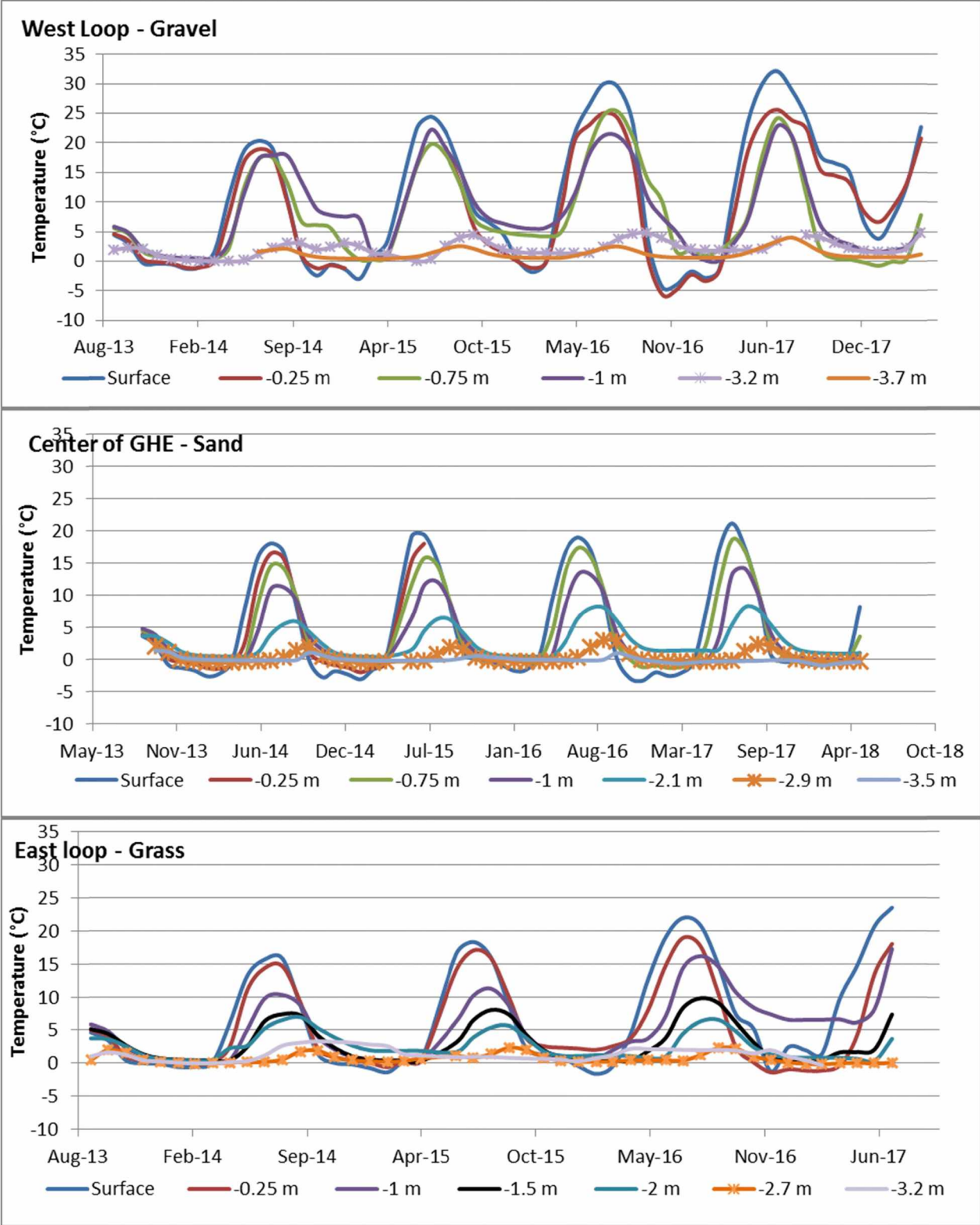
Figure 2.14. In-ground temperatures over time. The starred lines are the closest to the GHE coils. This point has failed in the gravel, but the rest of the points are all generally warmer than the grass and sand. Incomplete data sets indicate a failed sensor.
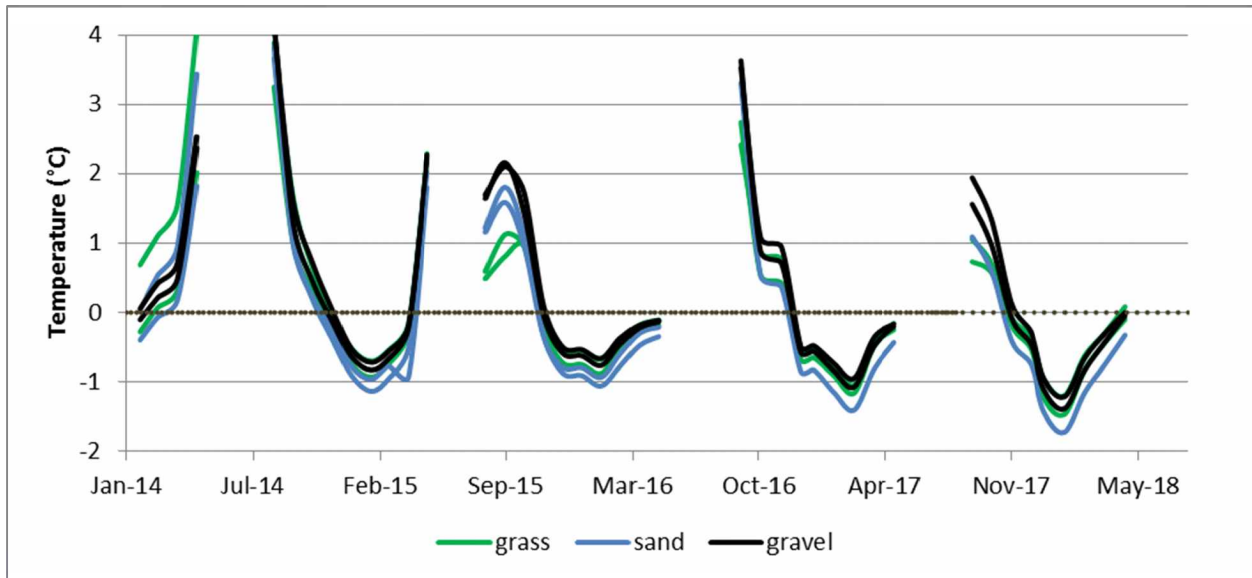
Figure 2.15. Temperatures of the fluid returning from the GHE. The temperatures in the beginning of 2014 do not have the effects of the summer on the surface treatments as the system was not complete until September 2013. Holes in the data are due to no fluid returning to the building because the system is off in the summer.

2.6.4 Heat delivered

The heat delivered to the building was tracked along with the electrical use of the heat pump. Heat delivered is presented in Table 2.7. Knowing the heat delivered and the electrical input allows for the calculation of the energy removed from the GHE shown in Table 2.8 (the GHE flow and temperature meter was unable to accurately record the energy removal from the ground directly). The higher electrical use but roughly the same amount of heat delivered to the building during the third winter is an indication of the loss in efficiency. Year 1 does not include a full year of data so it is not easily comparable. In addition, the masonry stove was fired on a regular basis during year one, offsetting the heat load.

Table 2.7. Heat delivered

	Year 1 (winter 2013-14)		Year 2 (winter 2014-15)		Year 3 (winter 2015-16)		Year 4 (winter 2016-17)	
	Electric Use (kWh)	Energy Delivered (kWh)	Electric Use (kWh)	Energy Delivered (kWh)	Electric Use (kWh)	Energy Delivered (kWh)	Electric Use (kWh)	Energy Delivered (kWh)
Aug.	-	-	-	-	13	46	-	-
Sept.	-	-	129	537	154	543	146	342
Oct.	-	-	229	892	433	1,451	803	2051
Nov.	97	379	885	3,216	1,332	4,123	1,370	4479
Dec.	1,115	3,870	971	3,479	1,871	5,517	2,133	6593
Jan.	962	3,405	1,636	5,210	1,104	3,250	2,096	5589
Feb.	908	3,167	1,272	3,966	1,129	3,368	1,471	3932
Mar.	306	1,145	740	2,347	593	1,677	1,442	3816
April	297	1,109	132.	419	272	758	286	699
May	24	96	14	32	39	144	83	228
June	-	-	9	0	-	-	-	-
July	-	-	5	0	-	-	-	-
Total	3,709	13,171	6,022	20,098	6,946	20,877	9,832	27,729

Table 2.8. Energy extracted from the ground.

	Year 1 (winter 2013-14) Energy from Ground (kWh)	Year 2 (winter 2014-15) Energy from Ground (kWh)	Year 3 (winter 2015-16) Energy from Ground (kWh)	Year 4 (winter 2016-17) Energy from Ground (kWh)
Aug.	-	-	33	-
Sept.	-	408	389	196
Oct.	-	663	1,018	1,248
Nov.	282	2,331	2,791	3,109
Dec.	2,755	2,508	3,646	4,460
Jan.	2,443	3,574	2,146	3,493
Feb.	2,259	2,694	2,239	2,461
Mar.	839	1,607	1,084	2,374
April	812	287	486	413
May	72	18	105	145
June	-	-	-	-
July	-	-	-	-
Total	9,462	14,090	13,937	17,899

33

2.6.5 COP

The efficiency of the heat pump varied over the course of each heating season. It tended to be higher in the fall when the GHE was the warmest and decrease throughout the winter. However, as the heating demand of the building lessened in the spring, the COP improved as the heat pump delivered lower temperature heat to the building. Monthly COPs are presented in Table 2.9 while Figure 2.16 shows the trend for the COP. COP is calculated by taking the sum of the heat delivered to the building and dividing it by the sum of the electricity used by the heat pump over that time period.

Table 2.9. Heat pump COP.

	Year 1 (winter 2013-14)	Year 2 (winter 2014-15)	Year 3 (winter 2015-16)	Year 4 (winter 2016-17)
September		4.15	3.52	2.34
October		3.9	3.34	2.55
November	3.9	3.63	3.09	3.27
December	3.47	3.58	2.95	3.09
January	3.54	3.18	2.94	2.67
February	3.48	3.12	2.98	2.67
March	3.73	3.17	2.82	2.65
April	3.73	3.17	2.78	2.44
Annual	3.69	3.34	3.01	2.82
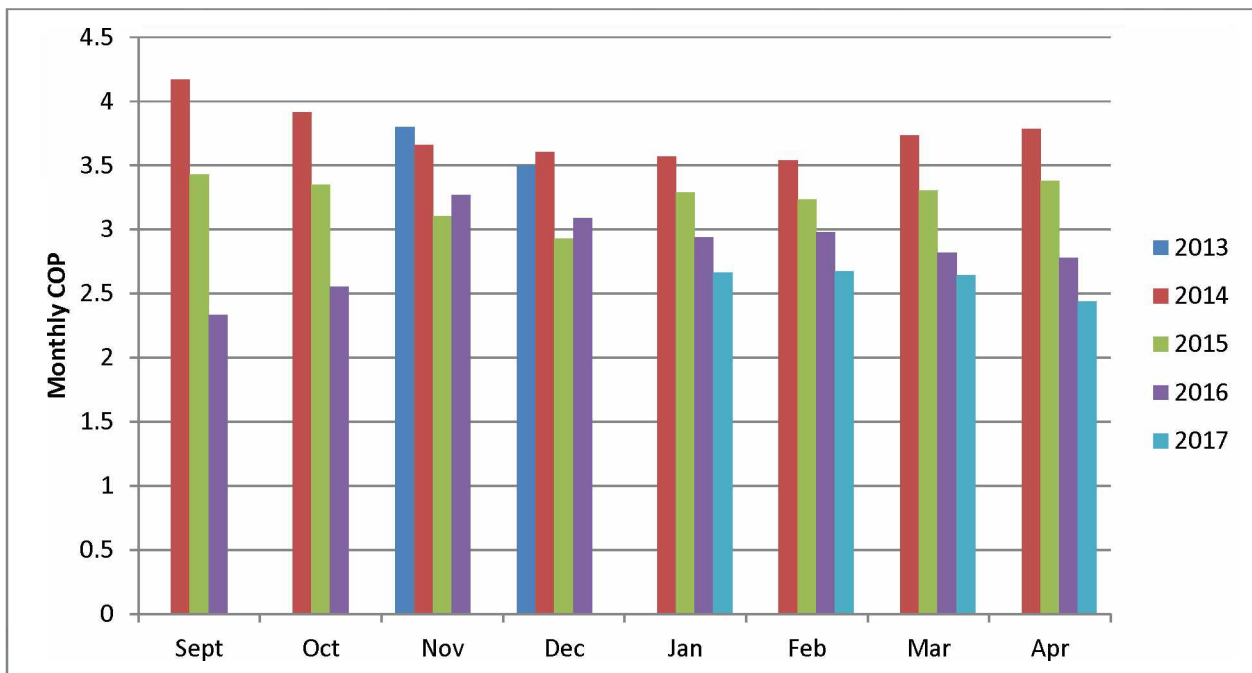
Figure 2.16. Heat Pump COP over time. The efficiency of the heat pump system degraded as the ground temperature decreased.

34

The COP for the heat pump is trending lower over time, with a 24% decline in the annual COP over 4 years. The average decline has not varied much with a 9.4% decline in the first 2 years, at 9.8% between the second and third winter, and dropping only 6.3% between the third and fourth winters. The severity of the winter can affect the efficiency of the heat pump, with lower outside temperatures calling for higher delivery fluid. Heating degree days (HDD) is a measure of demand for heat in a building and is dependent on outside temperature. HDD can be used to judge the severity of a winter in comparison to other years. Table 2.10 provides a comparison of the HDD for the heat pump study. Year 4 was the most severe winter with almost 1,000 more HDD than Year 3. This more extreme heating demand could factor into the lower COP in year 4.

Table 2.10. Heating degree days.

	Year 1 (winter 2013-14)	Year 2 (winter 2014-15)	Year 3 (winter 2015-16)	Year 4 (Winter 2016-2017)
°C HDD$_{18}$	6,921	6,769	6,487	7,535

2.7 Discussion

It was expected that the COP of this system would degrade over time until it reached an equilibrium state where the COP leveled out. Models predicted the equilibrium state to be reached after the 5th heating season [9]. The system has operated another 2 heating seasons since this data was evaluated. There have been some changes in the soils around the GHE that may be affecting the system more than the heat pump. When the system was installed there was flowing groundwater about 4.5 m below the surface, 1.5 m below the GHE. The level of the ground water has risen drastically in the past 2 years; it is now around 1.5 m below the surface, which means the GHE is potentially resting in moving ground water. The ground water could improve the system efficiency with higher temperature and better heat transfer.

Initial data analysis from the 2017-2018 heating season seemed to support improved efficiency (Figure 2.17). The 20% jump in COP during the 5th heating season was unexpected and may be due to several factors: a warmer winter, more use of the masonry stove, and changes in the ground water. There were no changes on the supply side of the heat pump; all the flows and delivery temperatures were the same for all 5 years.
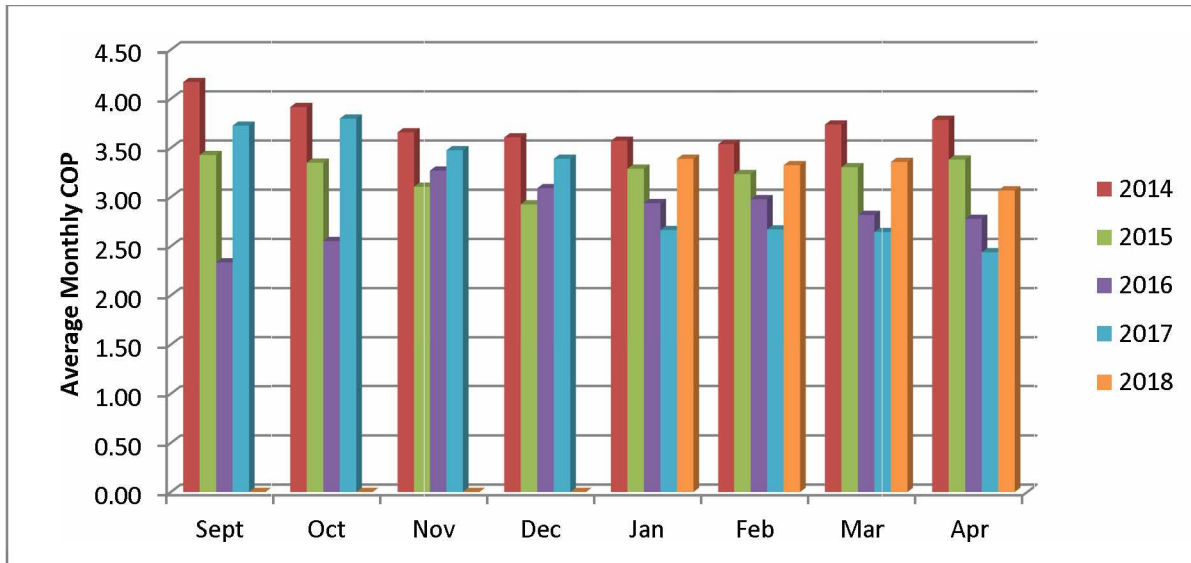
Figure 2.17. Heat Pump COP over time. The efficiency of the heat pump system was degrading until the 5th heating season.

If the ground water were improving the heat pump COP the return fluid temperature from the GHE would be higher, however it was slightly colder in year 5 than the previous four years (Figure 2.18).
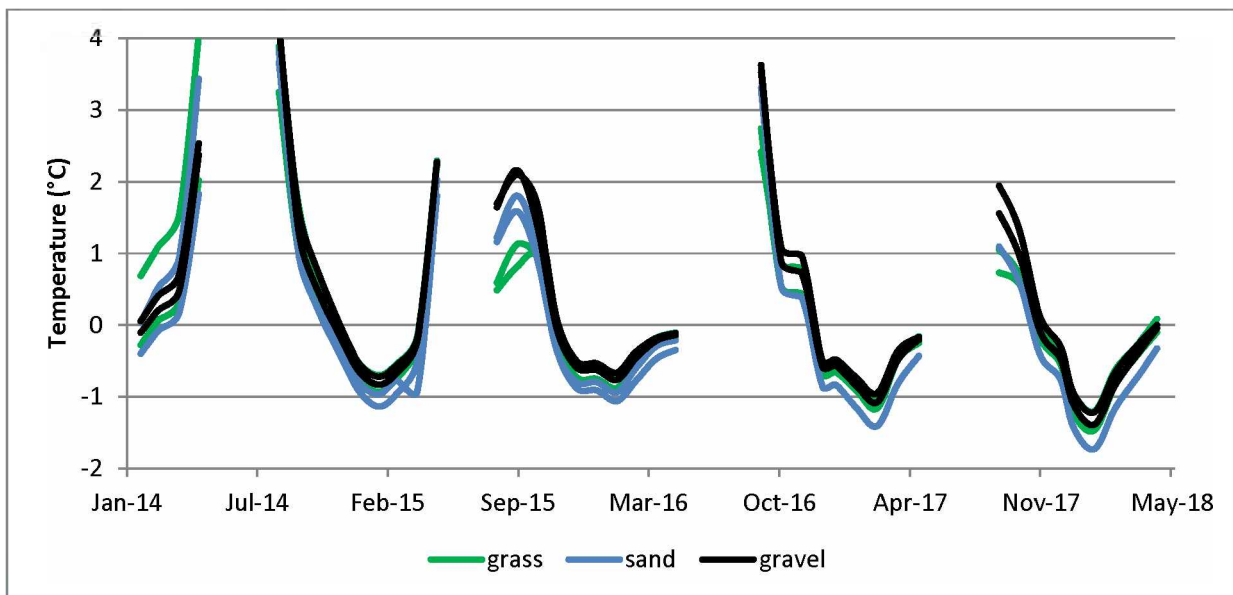
Figure 2.18. Temperatures of the fluid returning from the GHE. The trend is consistently down over the last 3 seasons.

The severity of the winter could affect the efficiency of the heat pump, with lower outside temperatures calling for higher delivery fluid. Table 2.11 provides a comparison of the HDD for the heat pump study. Year 4 was the most severe winter with almost 1,000 more HDD than Year

3. This more extreme heating demand could also factor into the lower COP in year 4, while lower demand in year 5 may contribute to a higher COP in that winter.

Table 2.11. Heating degree days.

	Year 1 (winter 2013-14)	Year 2 (winter 2014-15)	Year 3 (winter 2015-16)	Year 4 (winter 2016-17)	Year 5 (winter 2017-18)
°C HDD_{18}	6,921	6,769	6,487	7,535	6,667

The wood burning masonry stove provides heat to the same area as the GHSP. Its use is variable from winter to winter (based on building staff). Year 5 saw more wood burning than year 4. Table 2.12 shows a summary of the wood energy added to the building for each winter. As You et al. [10] point out supplemental heating systems can help the longevity of the GHE by lowering the amount of heat extracted from the GHE in a year. There was more wood burned in year 5 when compared to year 4 and less heat was extracted in year 5 from the ground (see Table 2.13.).

Table 2.12. Masonry stove use by year.

	Year 1 (winter 2013-14)	Year 2 (winter 2014-15)	Year 3 (winter 2015-16)	Year 4 (winter 2016-17)	Year 5 (winter 2017-18)
Wood Used (kWh)	7,139	10.9	5,578	2,873	5,023

Table 2.13 shows the energy sources for the heat pump system by year. It is interesting to note that year 4 and 5 extract almost the same amount of energy from the ground but year 4 used 2,208 more kWh of electrical energy than year 5. This extra electrical energy is not completely explained by lower GHE temperatures, or colder weather, or increased auxiliary heater use. It is possible that there was something mechanical in the heat pump that caused Year 4 to have such a low efficiency.

Table 2.13. Energy comparison by year.

	Year 1 (winter 2013-14)	Year 2 (winter 2014-15)	Year 3 (winter 2015-16)	Year 4 (winter 2016-17)	Year 5 (winter 2017-18)
Annual energy from the ground (kWh)	9,459	14,086	13,931	17,897	17,229
Annual Electricity Used (kWh)	3,709	6,022	6,941	9,832	7,624
Total Heat Delivered (kWh)	13,171	20,098	20,877	27,729	24,853

The heat pump failed early in the 2018-2019 season. It had no efficiency at startup in September 2018 and eventually shut down. Multiple visits by the installer and refrigerant technician found that the Thermostatic Expansion Valve (TXV) had failed and needed to be replaced. Once the valve was replaced the heat pump was still performing poorly; the system was run in reverse to flush the refrigerant through the filter. A TXV failure can produce failure bits that can impede the function of the refrigerant cycle. Once the system was well flushed it performed better. Data from the 2018-2019 season has not been evaluated yet. Further study of the failure of the TXV and a closer analysis of the Year 6 performance are necessary to determine whether Year 4 or Year 5 data is the anomaly in efficiency.

2.8 Conclusions and Recommendations

The original Meyer et al.[1] report found that a GSHP with a COP of 2.5 or greater would be cost effective in Fairbanks (based on $2.87 per gallon heating oil and $0.17/kWh electricity)[1]. That being said, the cost effectiveness of a GSHP depends on the cost of oil versus electricity, which has not been favorable to GHSPs since 2016 in Fairbanks.

The COP for the heat pump was trending lower over time; with a 24% decline in the annual average over the first 4 years. The decline in COP slowed slightly in year 4 from 9% down to 6%, this potentially indicates stabilization in the near future. Modeling suggests that the decline will level out around year 5 [11]. Changes in the groundwater may also be affecting the ground temperature and heat pump COP; future study will focus more on the groundwater factor.

Four years of operation is certainly not long enough to see all the changes the heat pump will create in the soil thermal regime. This heat pump demonstration will be monitored for at least another 6 years to verify the degradation in the soil temperatures and the COP.

2.9 Nomenclature

GSHP   Ground Source Heat Pump

CCHRC   Cold Climate Housing Research Center

RTF   Research and Testing Facility

GHE   Ground Heat Exchanger

UAF   University of Alaska Fairbanks

TC   Thermal Conductivity test

IGSHPA   International Ground Source Heat Pump Association

$°C \, HDD_{18}$ Heating degree days based on 18°C

TXV   Thermostatic Expansion Valve

COP   Coefficient of Performance

2.10 References

[1] J. Meyer, D. Pride, J. O'Toole, C. Craven, and V. Spencer, "Ground-source heat pumps in cold climates," Denali Commission, Fairbanks, AK, 2011.

[2] R. Garber-Slaght, C. Craven, R. Peterson, and R. Daanen, "Ground source heat pump demonstration in Fairbanks , Alaska," Cold Climate Housing Research Center, 2017.

[3] *2017 ASHRAE Handbook Fundamentals*. Atlanta: ASHRAE, 2017.

[4] Shannon & Wilson Inc., "Geotechnial design review proposed UAF/new Geist Road access Fairbanks, Alaska," Alaska Department of Transporation and Public Works, 31-1-01714-001. 2002.

[5] IGSHPA, *Ground source heat pump residential and light commercial design and installation guide*. Stillwater, OK: International Ground Source Heat Pump Association, 2009.

[6] G. Mueller and J. Zarling, "Ground source heat pump monitoring," Matanuska Electric Association, Inc., 1996.

[7] H. Nielson and J. Zarling, "Ground source heat pump demonstration," Alaska Energy Center, AEC 81-005-1, Fairbanks, AK, 1983.

[8] R. Garber-Slaght and V. Stevens, "Ground source heat pumps in Interior Alaska lessons learned from installed systems," Cold Climate Housing Research Center, Fairbanks, AK, 2014.

[9] R. Garber-Slaght and R. Peterson, "Can ground source heat pumps perform well in Alaska?," in *Proceedings of the IGSHPA Technical/Research Conference and Expo 2017*, 2017.

[10] T. You, W. Wu, W. Shi, B. Wang, and X. Li, "An overview of the problems and solutions of soil thermal imbalance of ground-coupled heat pumps in cold regions," *Appl. Energy*, vol. 177, pp. 515–536, 2016.

[11] R. Garber-Slaght, R. Daanen, and A. Roe, "Ground source heat pump efficiency in cold climates," *ASHRAE Trans.*, vol. 120, no. 2, 2014.

Chapter 3: Analytical Study of a Cold Climate Ground Source Heat Pump with Al_2O_3 Nanofluid in the Ground Heat Exchanger

3.1 Introduction

The common strategy for a ground source heat pump (GSHP) to work for a long time in a cold climate like Fairbanks, Alaska it to oversize the ground heat exchanger (GHE) [1]. This results in higher installation costs and pumping power. If there were a way to achieve similar GSHP performance with a smaller GHE there are potential install and pumping power savings. One possible way to have a smaller GHE is to improve the heat transfer capacity of the GHE fluid. This chapter evaluates nanofluids as a potential alternative heat transfer fluid for a smaller GHE through the use of theoretical calculations to determine thermophysical properties of a potential nanofluid with a methanol/water base.

3.2 GSHP Fluid Properties

The CCHRC GSHP uses a 20% methanol/water mixture in its ground loop. The methanol is necessary because the fluid is usually around 0°C and below in the winter. Satti [2] categorized the properties of this particular methanol mix at 0°C; they are presented in Table 3.1. The second row of Table 3.1 uses chemical equations for mixtures (equations (3.1)-(3.4) [3]) as a verification of Satti's numbers. With the exception of viscosity Satti's values are within 10% of expected generic values from the mixture equations and acceptable for this analytical study. Since viscosity is the pivotal factor in the thermophysical property calculations the value from equation (3.3) was judged a better estimate than Satti's for this analytical study.

Table 3.1. 20:80 Methanol/Water Properties at 0°C.

Source	Density	Specific Heat	Viscosity	Thermal Conductivity
	kg/m3	J/kg K	Pa s	W/m K
Satti, 2015 [2]	986	3631	0.00234	0.496
Equations 3.1-3.4	962	3913	0.00163	0.501
% Difference	2.5%	7.2%	44%	1.1%

$$\rho_{mix} = \rho_{methanol}\emptyset + \rho_{water}(1-\emptyset) \tag{3.1}$$

$$C_{pmix} = \frac{\rho_{methanol}C_{pmethanol}\emptyset + \rho_{water}C_{pwater}(1-\emptyset)}{\rho_{mix}} \tag{3.2}$$

41

$$\mu_{mix=}\frac{\rho_{methanol}\mu_{methanol}\emptyset+\rho_{water}\mu_{water}(1-\emptyset)}{\rho_{mix}} \qquad (3.3)$$

$$k_{mix=}\frac{\rho_{methanol}k_{methanol}\emptyset+\rho_{water}k_{water}(1-\emptyset)}{\rho_{mix}} \qquad (3.4)$$

The fluid flow in the ground heat exchanger (GHE) is relativity steady at 62 l/min. The temperatures to and from the GHE change from year to year, but also over the course of the heating season. As energy is extracted from the GHE the temperature drops until it reaches just below 0°C where the heat pump is extracting the energy of phase change and ice is created in the GHE. Summer heat and rain add energy back into the ground raising the temperature at the beginning of the heating season. Table 3.2 shows the incoming and exiting GHE temperatures as monthly averages. The average for all heating seasons has been -1.1°C; since it is impossible to get liquid water properties at this temperature, water properties were taken at 0°C liquid state close to -1.1°C.

Table 3.2. Monthly Average Fluid Temperatures from the Ground Loop.

	Average Fluid Temperature (°C)		Average Fluid Temperature (°C)
Feb. 2014	-1.61	Nov. 2015	-1.41
March 2014	-1.42	Dec. 2015	-1.83
April 2014	-1.10	Jan. 2016	-1.85
May 2014	0.95	Feb. 2016	-2.27
Sept. 2014	1.80	March 2016	-1.81
Oct. 2014	-0.46	April 2016	-2.29
Nov. 2014	-1.18	May 2016	-3.26
Dec. 2014	-1.63	Sept. 2016	2.63
Jan. 2015	-2.09	Oct. 2016	-0.15
Feb. 2015	-2.28	Nov. 2016	-0.22
March 2015	-2.14	Dec. 2016	-1.73
April 2015	-1.80	Jan. 2017	-1.69
May 2015	0.11	Feb. 2017	-2.00
Aug. 2015	-0.35	March 2017	-2.24
Sept. 2015	0.13	April 2017	-1.60
Oct. 2015	-0.18	May 2017	-1.09

3.3 Nanofluid Properties

There is the potential to shrink the size of the GHE if a fluid with better heat transfer is used as the energy collection medium. Nano materials can be added to the methanol mixture to improve the heat transfer. When nano materials are added to a fluid in small concentrations (up to 4%) the heat transfer can be improved by up to 30% in some applications [4].

In order to analyze the improved heat transfer of the nanofluid it is necessary to have accurate material properties of the nanofluid. There is a great deal of research into calculating the properties of nanofluids with different base fluids, however there is nothing readily available on 20% methanol as the base fluid. The properties of 20:80 methanol/water M/W were compared to water, 60:40 propylene glycol/water (PG/W), and 60:40 ethylene glycol/water (EG/W) (Figure 3.1). Methanol is closest to water for all four properties so equations using water as the base fluid would be used to develop properties for the methanol based nanofluid. However, such equations are not evaluated below 0°C. For the purposes of this thesis a mixture of equations developed for 60:40 ethylene glycol/water base fluid and water base fluid will be used.
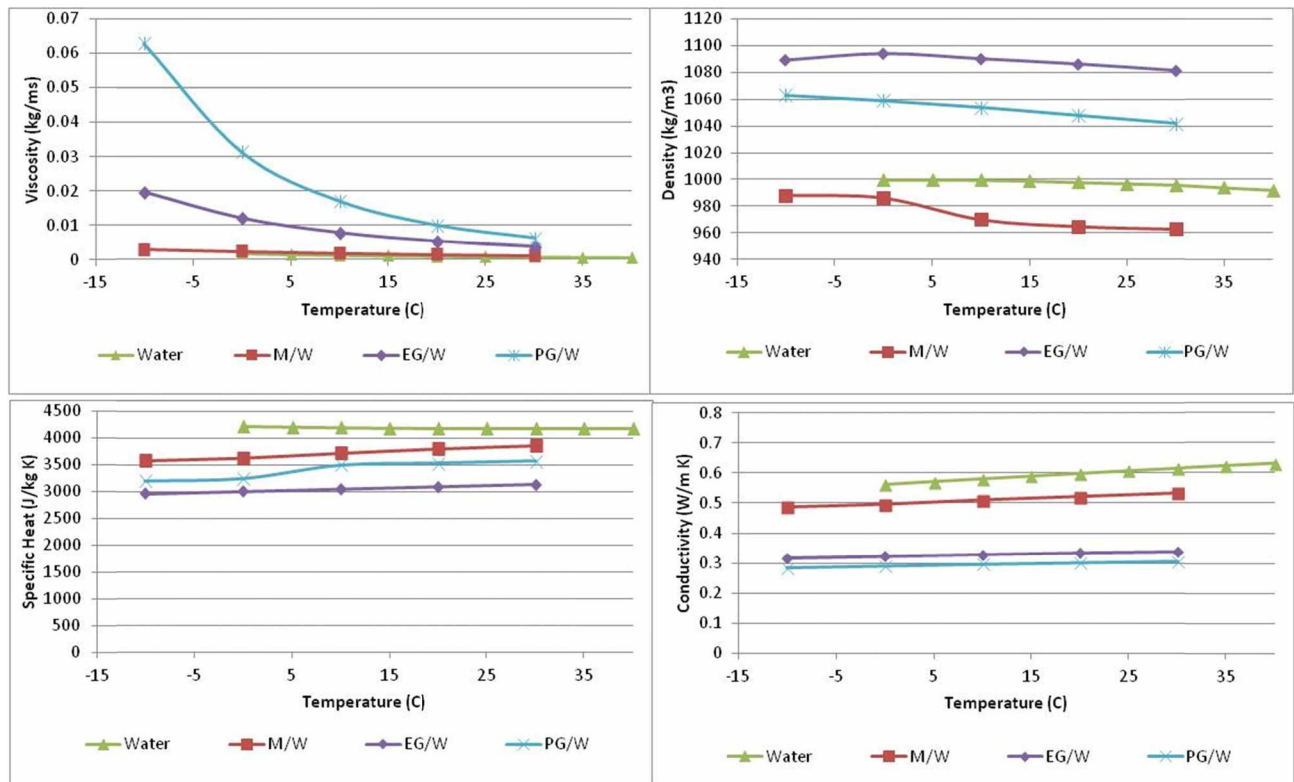
Figure 3.1. Thermophysical properties of heat transfer fluids. M/W is 20% methanol and 80% water. EG/W is 60% ethylene glycol and 40% water. PG/W is 60% propylene glycol and 40% water.

Al_2O_3 and CuO nanoparticles were evaluated to see how they might improve the thermal transfer of the methanol/water mixture. Particle concentration increments up to 6% were evaluated to determine which might be optimal for heat transfer, pumping power and cost. Al_2O_3 has a density of 3600 kg/m³, thermal conductivity of 36 W/m·K and specific heat of 765 J/kg·K [5]. CuO has a density of 6500 kg/m³, thermal conductivity of 18 W/m·K and specific heat of 533 J/kg·K [5].

In order to determine the density of a nanofluid mixture the Cheremisinoff/Pak and Cho [6] equation (3.5) for density has been found to accurately calculate the density of a variety of nanofluids with different base fluids; including water, 60:40 EG/W and 60:40 PG/W [7]. Satti et al. [7] found the theoretical calculation to be within 4% of several nanofluids with an EG/W base between 0°C and 90°C.

$$\rho_{nf=}\rho_p\emptyset + \rho_{bf}(1 - \emptyset) \tag{3.5}$$

Vajjha and Das [8] developed an equation (3.6) for the viscosity of nanofluids between 0°C and 90°C. This is for EG/W as a base fluid with Al_2O_3 or CuO as nanoparticles.

$$\frac{\mu_{nf}}{\mu_{bf}} = A_1 e^{A_2\emptyset} \tag{3.6}$$

A_1=0.983 for Al_2O, A_1=0.9197 for CuO

A_2=12.959 for Al_2O_3, A_2=22.8539 for CuO

Viscosity is a strong function of temperature so an equation for temperatures closer to the -3°C to 3°C range is desirable. There is not temperature term in this equation; however, the temperature dependent viscosity of the base fluid is taken into account in the μ_{bf} term.

The thermal conductivity of the fluid can be greatly enhanced by the addition of nanoparticles. The conductivity of the base fluid and the particles as well as the concentration of the particles are the major factors in calculating the conductivity of the nanofluid. Additionally, there is a contribution of Brownian motion of nano particles to the conductivity. The Hamilton and Crosser equation for the thermal conductivity of micro particles is the foundation for nanofluids calculations. It is the first term in the Vajjha & Das [5] equation (3.7a). The second term is to account for Brownian motion. Koo and Kleinstreuer [9] have a similar equation but

44

their concentrations are less than 1% therefore the Vajjha and Das equation (3.7) was used for this project. None of the discussed equations are verified in the temperature range for the ground fluid but since the thermal conductivity is a stronger function of particle concentration it is expected the Vajjha and Das [5] equation (3.7) (from 25°C to 90°C) provides a closer approximation.

$$k_{nf} = \frac{k_p + 2k_{bf} - 2(k_{bf} - k_p)\emptyset}{k_p + 2k_{bf} + (k_{bf} - k_p)\emptyset} k_{bf} + 5*10^4 \left(\beta \emptyset \rho_{bf} C_{pbf} \sqrt{\frac{KT}{\rho_p d_p}} \right) f(T,\emptyset) \qquad \textbf{(3.7a)}$$

$$\beta = 8.4407(100\emptyset)^{-1.07304} \text{ for } Al_2O_3; \beta = 9.881(100\emptyset)^{-0.9446} \text{ for } CuO \qquad \textbf{(3.7b)}$$

$$f(T,\emptyset) = (2.8217*10^{-2}\emptyset + 3.917*10^{-3}) \left(\frac{T}{T_o} \right) + (-3.0669*10^{-2}\emptyset - 3.91123*10^{-3})$$

$$\textbf{(3.7c)}$$

Xuan and Roetzel [10] presented a theoretical equation (3.8) for specific heat which compares well to experimental data [4].

$$C_{pnf} = \frac{\emptyset \rho_p C_{pp} + (1-\emptyset)\rho_{bf} C_{pbf}}{\rho_{nf}} \qquad \textbf{(3.8)}$$

3.5 Heat Transfer and Pumping Power Calculations

Equations for the Reynolds number (Re) (3.9), the Prandtl number (Pr) (3.10), the Nusselt number (Nu) (3.11), and the convective heat transfer coefficient (h) (3.11) are well known and often used equations [11]

$$Re = \frac{Vd\rho}{\mu} \qquad \textbf{(3.9)}$$

$$Pr = (\mu C_p)/k \qquad \textbf{(3.10)}$$

For pure liquids the Gnielinski equation is most widely used to calculate the Nusselt number [11]

$$Nu = 0.012(Re^{0.87} - 280)Pr^{0.4} = \frac{hD}{k} \qquad \textbf{(3.11)}$$

Vajjha and Das [4] developed a Nusselt number equation (3.12) for nano fluids in turbulent flow that is based on Gnielinski.

$$Nu_{nf} = 0.065(Re_{nf}^{0.65} - 60.22)(1 + 0.0167\emptyset^{0.15})Pr_{nf}^{0.542} \qquad \textbf{(3.12)}$$

$$3000 < Re < 16,000, 0 < \emptyset < 0.06$$

The Churchilll correlations (3.13) for friction factor for turbulent flow in smooth pipes is used [12]

$$f = 8\left[\left(\frac{8}{Re_{D_h}}\right)^{12} + \frac{1}{(A+B)^{1.5}}\right]^{1/12}$$

(3.13a)

$$A = \left[2.457ln\left(\frac{1}{\left(7/Re_{D_h}\right)^{0.9} + (0.27\varepsilon/D_h)}\right)\right]^{16}$$

(3.13b)

$$B = \left(\frac{37,530}{Re_{D_h}}\right)^{16}$$

(3.13c)

The friction factor equations for nanofluids also comes from Vajjha and Das [4] (3.14).

$$f_{nf} = 0.3164Re_{nf}^{-0.25}\left(\frac{\rho_{nf}}{\rho_{bf}}\right)^{0.797}\left(\frac{\mu_{nf}}{\mu_{bf}}\right)^{0.108}$$

(3.14)

4000<Re<16,000; 0<φ<0.06

Equations for pressure loss and pumping power are from Bejan [11]. The pressure loss in a pipe can be found using equation (3.15).

$$\Delta P = \frac{fL\rho V^2}{2D}$$

(3.15)

The pumping power is calculated using equation (3.16).

$$W = \Delta PAV$$

(3.16)

3.6 Analytical Results

The thermal/fluid properties of Al_2O_3 nanoparticles in M/W base fluid were calculated using the above equations. The numerical results are presented in Table 3.3 and Table 3.4. All properties but specific heat increase with increasing concentration as shown in Figure 3.2 through Figure 3.5.

46

Table 3.3. Al$_2$O$_3$ nanofluid properties at 0°C.

Concentration	Density	Specific Heat	Viscosity	Thermal Conductivity
	kg/m3	J/kg K	Pa s	W/m K
20% Methanol with no particles	986	3631.08	0.00163	0.496
0.01	1012.14	3529.14	0.00182	0.509
0.02	1038.28	3432.33	0.00208	0.522
0.03	1064.42	3340.28	0.00236	0.536
0.04	1090.56	3252.64	0.00269	0.550
0.05	1116.70	3169.10	0.00306	0.564
0.06	1142.84	3089.38	0.00349	0.578

Table 3.4. CuO nanofluid properties at 0°C.

Concentration	Density	Specific Heat	Viscosity	Thermal Conductivity
	kg/m3	J/kg K	Pa s	W/m K
20% Methanol with no particles	986	3631.08	0.00163	0.496
0.01	1041.14	3437.68	0.00188	0.508
0.02	1096.28	3263.74	0.00237	0.5203
0.03	1151.42	3106.46	0.00298	0.532
0.04	1206.56	2963.55	0.00374	0.545
0.05	1261.7	2833.14	0.00470	0.557
0.06	1316.84	2713.64	0.00591	0.570

Figure 3.2. Thermal conductivity of Al$_2$O$_3$ and CuO nanoparticles in 20:80 methanol/water base fluid. The red square at 0 concentration is the thermal conductivity of M/W without nanoparticles.

Figure 3.3. Viscosity of Al$_2$O$_3$ and CuO nanoparticles in 20:80 methanol/water base fluid. The red square at 0 concentration is the viscosity of M/W without nanoparticles.

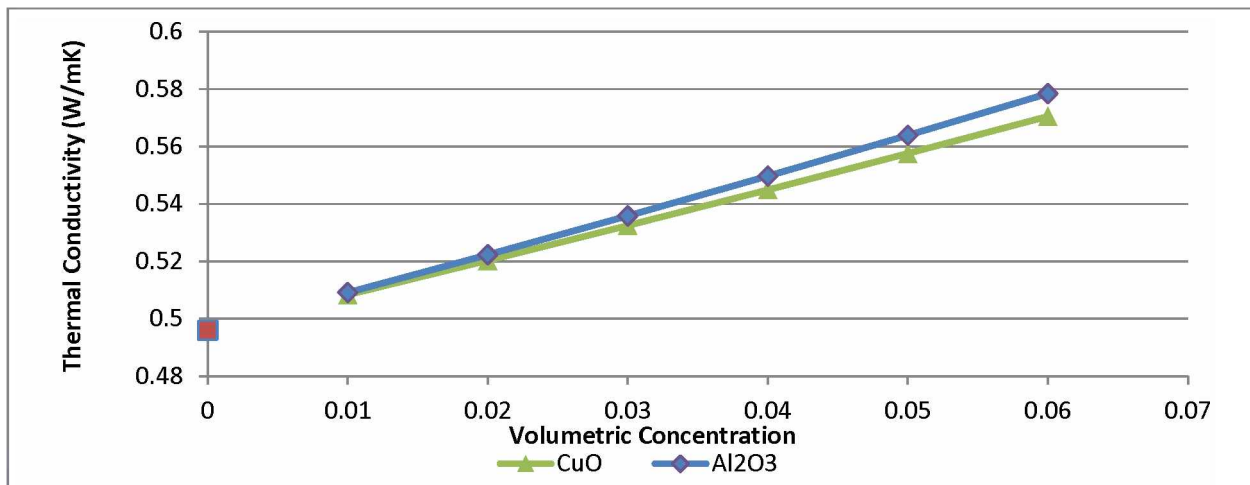**Figure 3.4. Density of Al$_2$O$_3$ and CuO nanoparticles in 20:80 methanol/water base fluid. The red square at 0 concentration is the density of M/W without nanoparticles.**
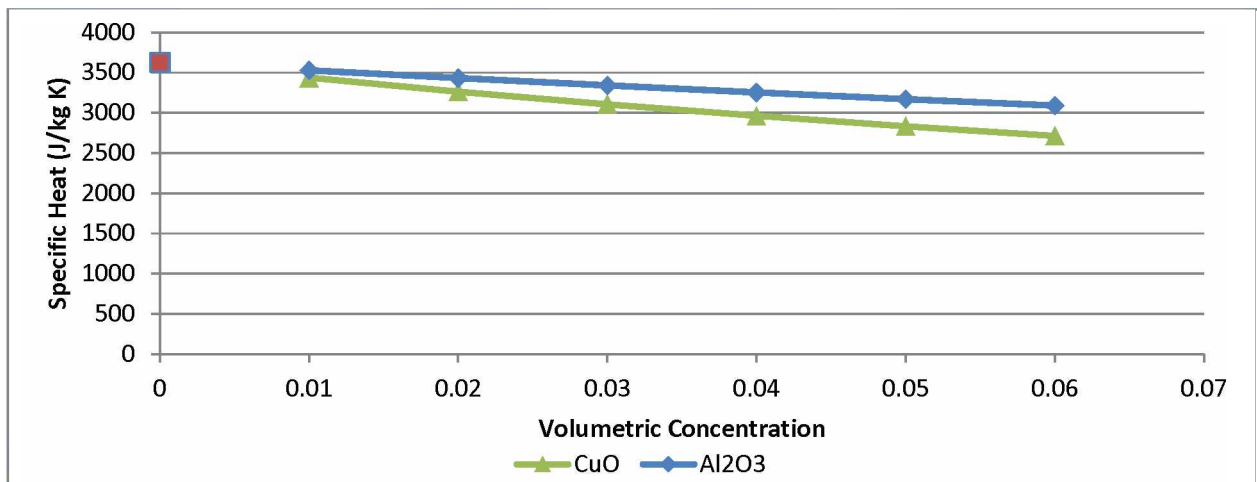
Figure 3.5. Specific heat of Al$_2$O$_3$ and CuO nanoparticles in 20:80 methanol/water base fluid. The red square at 0 concentration is the specific heat of M/W without nanoparticles.
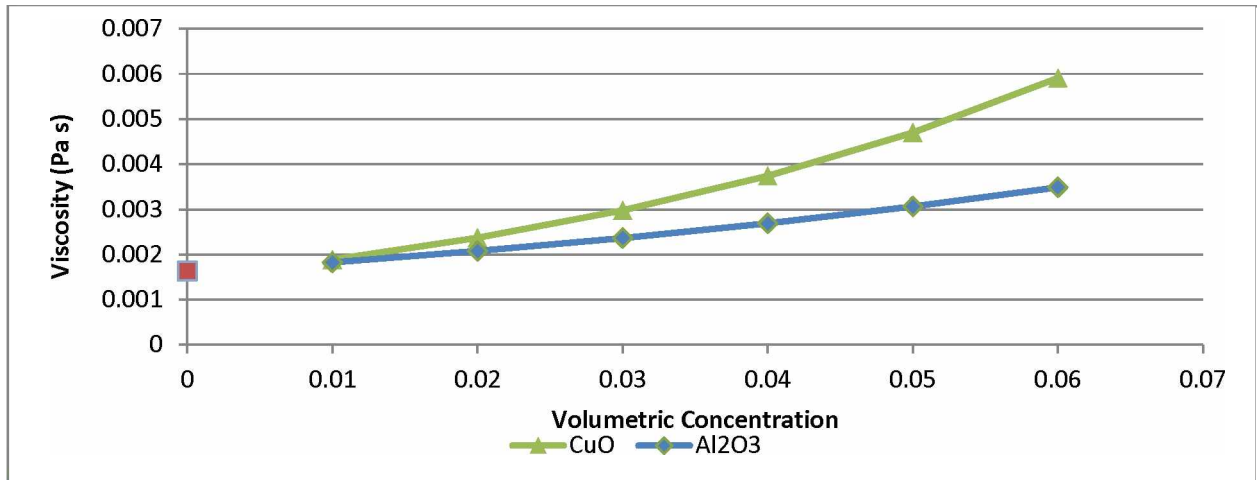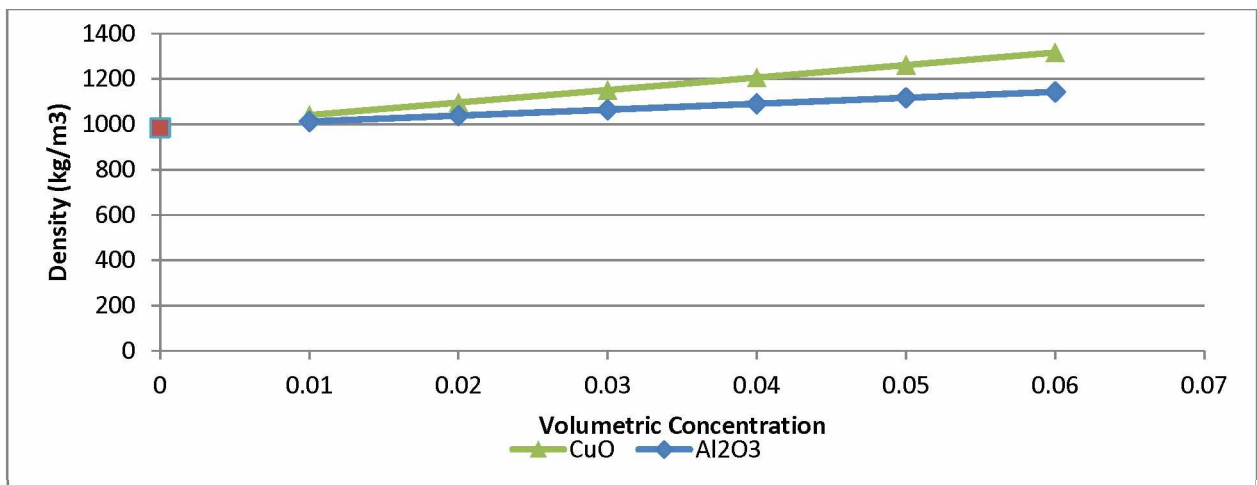
Table 3.5 presents the heat transfer properties for the Al_2O_3 nanofluid in the GHE. Figure 3.6 compares the heat transfer coefficient of the nanofluid at various concentrations to the heat transfer coefficient (h) value for 20:80 methanol/water at a velocity of 3.7 m/s, the current rate of the flow in the GHE. The addition of Al_2O_3 does not improve the heat transfer coefficient over the base fluid.

Table 3.5. Al_2O_3 Heat transfer properties.

Particle Concentration	Prandtl	Reynolds	Nusselt	Heat Transfer
				W/m^2K
20% Methanol with no particles	11.93	7069.88	64.18	1649.77
0.01	12.64	6485.48	62.28	1668.91
0.02	13.64	5844.34	59.65	1639.80
0.03	14.73	5263.25	57.01	1607.81
0.04	15.92	4737.08	54.37	1573.06
0.05	17.21	4261.06	51.74	1535.49
0.06	18.62	3830.77	49.11	1494.94

*The Nusselt number is calculated using Vajjha &Das [4] except for the pure methanol and water which uses the Gnielinski equation
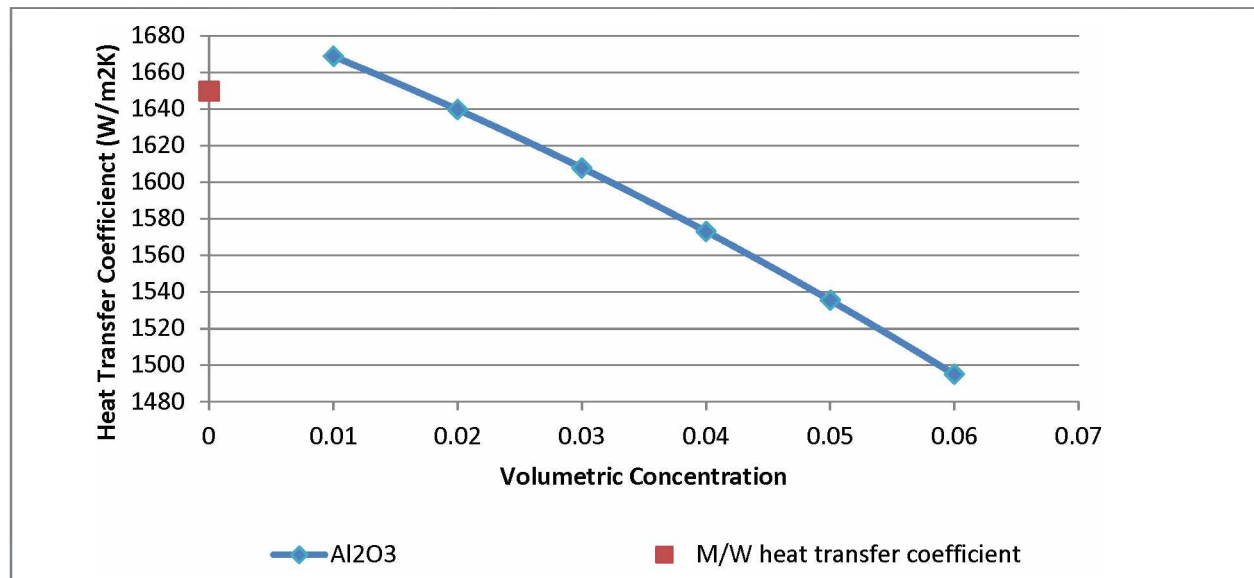
Figure 3.6. Heat transfer coefficient for Al_2O_3 nanofluid in methanol/water base fluid compared by concentration of particles.

The high flow rate combined with the low temperature create conditions where the addition of nano particles does not enhance the heat transfer very much. The low temperature of the fluid raises the viscosity to the point where there is no improvement in pumping power either. In fact, the pumping power of the nanofluid is higher than pure methanol (see Table 3.6).

Table 3.6. Pumping power for Al$_2$O$_3$ nanofluid.

Particle Concentration	Friction Factor*	Pressure Loss	Pumping Power
		Pa	W
20% Methanol with no particles	0.3456	497803.70	86.82
0.01	0.0364	537306.11	93.71
0.02	0.0387	585465.66	102.11
0.03	0.0411	637316.38	111.15
0.04	0.0436	693112.01	120.88
0.05	0.0463	753122.56	131.35
0.06	0.0491	817635.34	142.60

*The Friction Factor is calculated using Vajjha &Das [4] equation 3.14 except for the pure methanol and water which uses the Churchill equation 3.13.

CuO nanofluid does not perform better than Al$_2$O$_3$ in this analysis (see Table 3.7 and Figure 3.7).

Table 3.7. CuO heat transfer properties.

Particle Concentration	Prandtl	Reynolds	Nusselt	Heat Transfer
				W/m^{2}K
20% Methanol with no particles	11.93	7069.88	64.18	1649.77
0.01	12.74	6458.70	62.33	1667.62
0.02	14.85	5411.33	58.58	1604.11
0.03	17.36	4522.34	54.71	1533.43
0.04	20.34	3770.73	50.74	1455.29
0.05	23.88	3137.47	46.65	1369.01
0.06	28.10	2605.57	42.42	1273.73

Figure 3.7. CuO nanofluid heat transfer coefficient and pumping power estimate. Nano particle do not improve heat transfer or lower pumping power in this application.

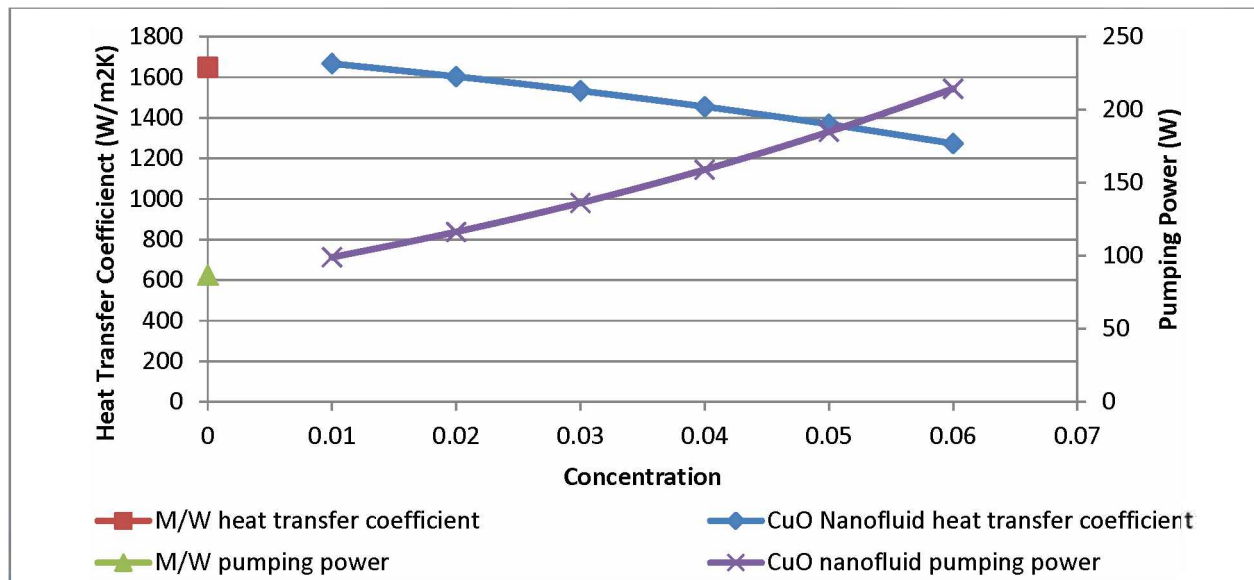## 3.7 Discussion

Nanofluids seem to perform better in the laminar range where the benefits of Brownian motion are more readily apparent [13]. This particular heat pump does not work well at flows lower than 45 l/min or 2.7 m/s. At this minimum flow for the heat pump the heat transfer coefficient of the nanofluids does not improve over methanol/water.

Slowing the flow down to the laminar region at 3 l/min creates a scenario where the heat transfer coefficient of the nanofluid is an improvement over the M/W base fluid (Figure 3.8). However, at this flow rate the existing heat pump cannot operate.
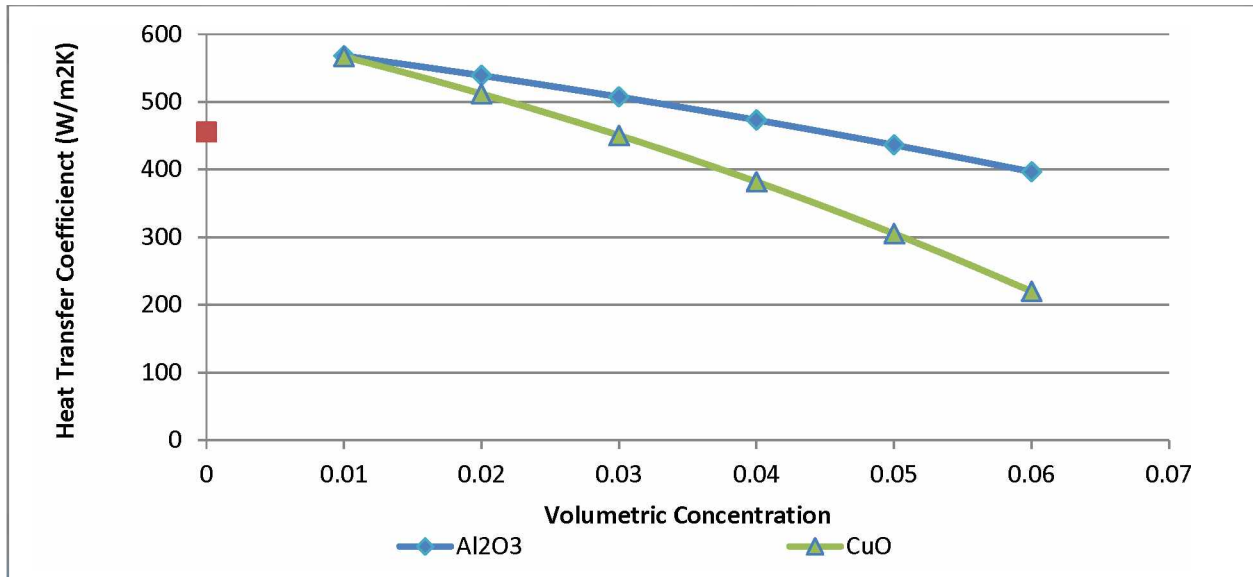
Figure 3.8. Heat transfer in the laminar range. Nanoparticles perform better in laminar flow.

3.8 Conclusions

Based on these analytical calculations Al_2O_3 and CuO in 20:80 methanol /water are not better option for heat transfer in the GHE of a cold climate heat pump system.

Regardless, there are other big questions that also need to be addressed: does the addition of nano particles change the corrosion potential of the methanol base fluid and is there any benefit in shrinking the size of the ground loop in a cold climate? Methanol is a highly corrosive fluid for heat transfer applications and mixtures used in heat pumps have corrosion inhibitors added. The corrosion potential of a methanol based nanofluid is unknown.

GSHPs work well in areas that have a balanced heating a cooling load. In a heating dominated climate they can extract more heat from the ground than is replaced in the summer months. In order to lessen this affect, ground loops in cold climates are oversized to provide

more mass from which to extract energy. A new fluid that could extract more heat would allow for a smaller GHE, but it may come at the cost of more rapid depletion of the energy from the ground. A carefully constructed model of the soils and the heat extraction loop will help understand this question.

3.9 Nomenclature

GSHP	Ground Source Heat Pump
M/W	20% water/80% methanol
PG/W	60% propylene glycol/40% water
EG/W	60% ethylene glycol/40% water
Nu	Nusselt number $\left(\frac{hD}{k}\right)$
Re	Reynolds number $(\frac{\rho VD}{\mu})$
Pr	Prandtl number $(\frac{c_p\mu}{k})$
c_p	Specific heat (J/kg·K)
k	Thermal conductivity (W/m·K)
h	Convective heat transfer coefficient (W/m^2·K)
K	The Stephan Boltzmann constant (1.381 x 1^{23} J/K)
d	Diameter (m)
T	Temperature (K)
T_o	Reference temperature (273 K)
f	Friction factor
L	Pipe length (m)
D	Pipe diameter (m)
A	Pipe area (m^2)
V	Velocity (m/s)

3.10 Greek Symbols

μ	Dynamic Viscosity (mPa·s)
ρ	Density (kg/m^3)
$\emptyset$	Volumetric concentration

3.11 Subscripts

nf	nanofluid
p	particle
bf	base fluid
mix	methanol and water
h	hydraulic

3.12 References

[1] W. Wu, B. Wang, T. You, W. Shi, and X. Li, "A potential solution for thermal imbalance of ground source heat pump systems in cold regions: ground source absorption heat pump," *Renew. Energy*, vol. 59, pp. 39–48, 2013.

[2] J. Satti, "Studies on Thermophysical Properties of Nanofluids and Their Application in Ground Source Heat Pump, a Dissertation," University of Alaska Fairbanks, 2015.

[3] R. C. Reid, J. M. Prausnitz, and T. Sherwood, *The Properties of Gases and Liquids*, 4th Editio. New York: McGraw Hill, 1987.

[4] R. S. Vajjha and D. K. Das, "A review and analysis on influence of temperature and concentration of nanofluids on thermophysical properties, heat transfer and pumping power," *Int. J. Heat Mass Transf.*, vol. 55, no. 15–16, pp. 4063–4078, 2012.

[5] R. S. Vajjha and D. K. Das, "Measurement of thermal conductivity of three nanofluids and development of new correlations," *Int. J. Heat Mass Transf.*, vol. 52, pp. 4675–4682, 2009.

[6] B. C. Pak and Y. I. Cho, "Hydrodynamic and heat transfer study of dispersed fluids with submicron metallic oxide particles," *Exp. Heat Transf.*, vol. 11, no. 2, pp. 151–170, 1998.

[7] J. R. Satti, D. K. Das, and D. R. Ray, "Measurements of Densities of Propylene Glycol-Based Nanofluids and Comparison With Theory," *J. Therm. Sci. Eng. Appl.*, vol. 8, no. 2, p. 021021, 2016.

[8] R. S. Vajjha and D. K. Das, *Measurements of thermophysical properties of nanofuids and computation of heat transfer characteristics*. Lambert Academic Publishing, 2010.

[9] J. Koo and C. Kleinstreuer, "Laminar nanofluid flow in microheat-sinks," *Heat Mass Transf.*, vol. 48, pp. 2652–2611, 2005.

[10] Y. Xuan and W. Roetzel, "Conceptions for heat transfer correlation of nanofluid," *Int. J. Heat Mass Transf.*, vol. 43, pp. 3701–3707, 2000.

[11] A. Bejan, *Heat Transfer*. John Wiley and Sons, 1993.

[12] *2017 ASHRAE Handbook Fundamentals*. Atlanta: ASHRAE, 2017.

[13] D. R. Ray, "Performance analysis of three nanofluids in liquid to gas and liquid to liquid heat exchangers," an M.S. thesis. Univeristy of Alaska Fairbanks, 2013.

Chapter 4: GSHP Soil Model

4.1 Introduction

The ground source heat pump (GSHP) demonstration at the Cold Climate Housing Research Center (CCHRC) has provided data on the soil interactions with the heat pump system for 6 seasons. This data is in the form of how much heat energy has been extracted from the ground heat exchanger (GHE), what the temperatures within the GHE have been, and the temperature of the fluid in the GHE loops. This data is useful in developing a soil model to evaluate the impacts of the GHE on the soil several years out from the current point. Additionally, a soil model can evaluate potential changes in the soil thermal/moisture regime and how those changes might impact the GSHP system. This model can also determine if the GHE can handle more heat extraction in the long term if CCHRC wanted to install a bigger heat pump to heat more of the building.

4.1.1 Past soil models for this heat pump

There are three Comsol Multiphysics models of this heat pump installation ([1]–[3]). Garber-Slaght et al. [1] developed a Comsol model of the project before the installation. The initial model informed the location and the spacing for the GHE. The GHE is installed in a field that is not plowed in the winter and the coils are 1.8 m apart, further apart than a typical installation in Fairbanks at the time (1.5 m). This initial model showed the temperature dropping in the first 4 years and permafrost developing by year 4 (Figure 4.1).
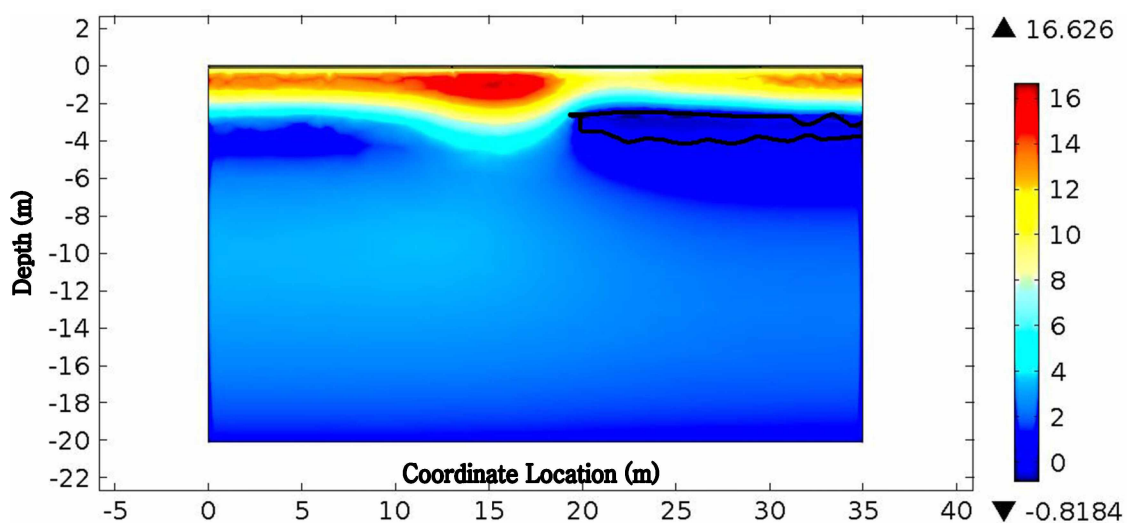

Figure 4.1. Profile from near the center of the simulation at the end of 4 years. The frozen area under the GHE is outlined in black [1]. The color legend is in °C.

55

This model used an estimate of heat demand based on outdoor air that overestimated the actual heat extraction. Figure 4.2 shows the modeled value for heat extraction with the actual daily average from the first four years of operation.
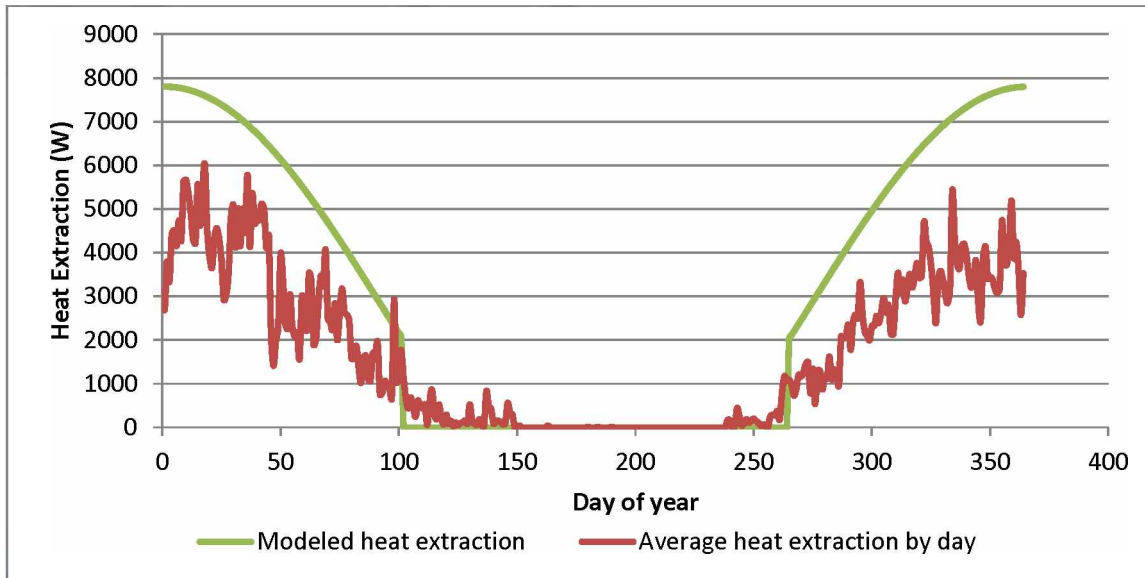

Figure 4.2. Modeled versus actual heat extraction. This initial model was designed conservatively to add a factor of safety to the GHE design [1].

Bishop [3] also developed a Comsol model of the GHE and surrounding soil. His model overestimated the heat extraction from the soil by three times the average heat extraction per year. He concluded that the system would fail to deliver adequate heat within 3 years, without active recharge of the soil. This has obviously not been the case.

Garber-Slaght and Peterson [4] completed a third Comsol model using the first 3 years of data from the installation. The heat extraction equation was very similar to Figure 4.2 the amplitude was lower brining it more in line with the daily averaged data. This model looked at optimum depth of GHE (approximately 2.5 m) for this location. It also evaluated the 10 year efficiency with a 50% higher heat extraction rate and found minimal change in the average COP over 10 years. This model shows the performance of the heat pump equilibrates after 5 years.

4.2 Software package

Temp/W$^{©}$ 2012 by GEO-SLOPE International Ltd. is an industry standard for geotechnical engineering. It is a 2-dimensional finite element modeling software. It was used in this thesis as a comparison to previous models and to focus on the thermal aspects of the soils around the GHE more. It was chosen after consultation with University of Alaska Professor Emeritus John

Zarling, who has done most of the heat pump studies in Alaska. Temp/W is a finite element software product that can model heat transfer through porous and solid materials while taking into account freezing and thawing actions. TEMP/W can be integrated with SEEP/W to analyze convective heat transfer in the soil, which was attractive due to the ground water movement at the site; however, SEEP/W was not integrated for this thesis; it is a future project.

4.2.1 Governing Equations

Conduction is the principal mechanism for heat flow in the Temp/W model [5]. It is governed by equation (4.1). Conductive heat flow is directly dependent on thermal conductivity and the temperature gradient.

$$q = -k \frac{\partial T}{\partial x} \tag{4.1}$$

The governing differential equation (4.2) states that the change in stored heat of an elemental volume is equal to the difference in heat flux entering and leaving the volume.

$$\frac{\partial}{\partial x}\left(k_x \frac{\partial T}{\partial x}\right) + \frac{\partial}{\partial y}\left(k_y \frac{\partial T}{\partial y}\right) + Q = \lambda \frac{\partial T}{\partial t} \tag{4.2}$$

The heat storage of an element is equal to the volumetric heat capacity of the material plus the latent heat associated with phase change (equation (4.3)).

$$\lambda = c_v + L \frac{\partial w_u}{\partial T} \tag{4.3}$$

4.3 Domain and Grid Layout

The CCHRC heat pump is installed in a field to the northwest of the research center. The GHE is roughly a rectangular box 15 m wide by 30.5 m long and 3 m deep (as installed it is mostly rectangular with an el in one corner due to site constraints). For a 2-dimensional model it is assumed infinite in its long direction and symmetric in its wide direction. Since it is symmetric, half of the GHE was developed in this model. The soils in and around the GHE are an important component of how the system performs so an extra soil was modeled on three sides of the GHE to show where the impact of the GHE on the soil ends. The full domain is 30 m deep and 19.5 m wide. Figure 4.3 shows the domain for the soil model. The line at 2.8 m is the line that the heat extraction coils are on, they are visible in this graphic as the 3 fat aqua lines that start at 1.5 m and proceed to the right. Each heat extraction coil is 1 m wide and 1. 8 m separates

the coils.

Figure 4.3 also shows the grid layout for the model. The global element size is 0.1m; however, the further from the surface and the GHE the larger the elements. The largest size is 1.5 m at the very bottom and right of the domain. There are 14,084 nodes and 14,091 elements in this mesh.
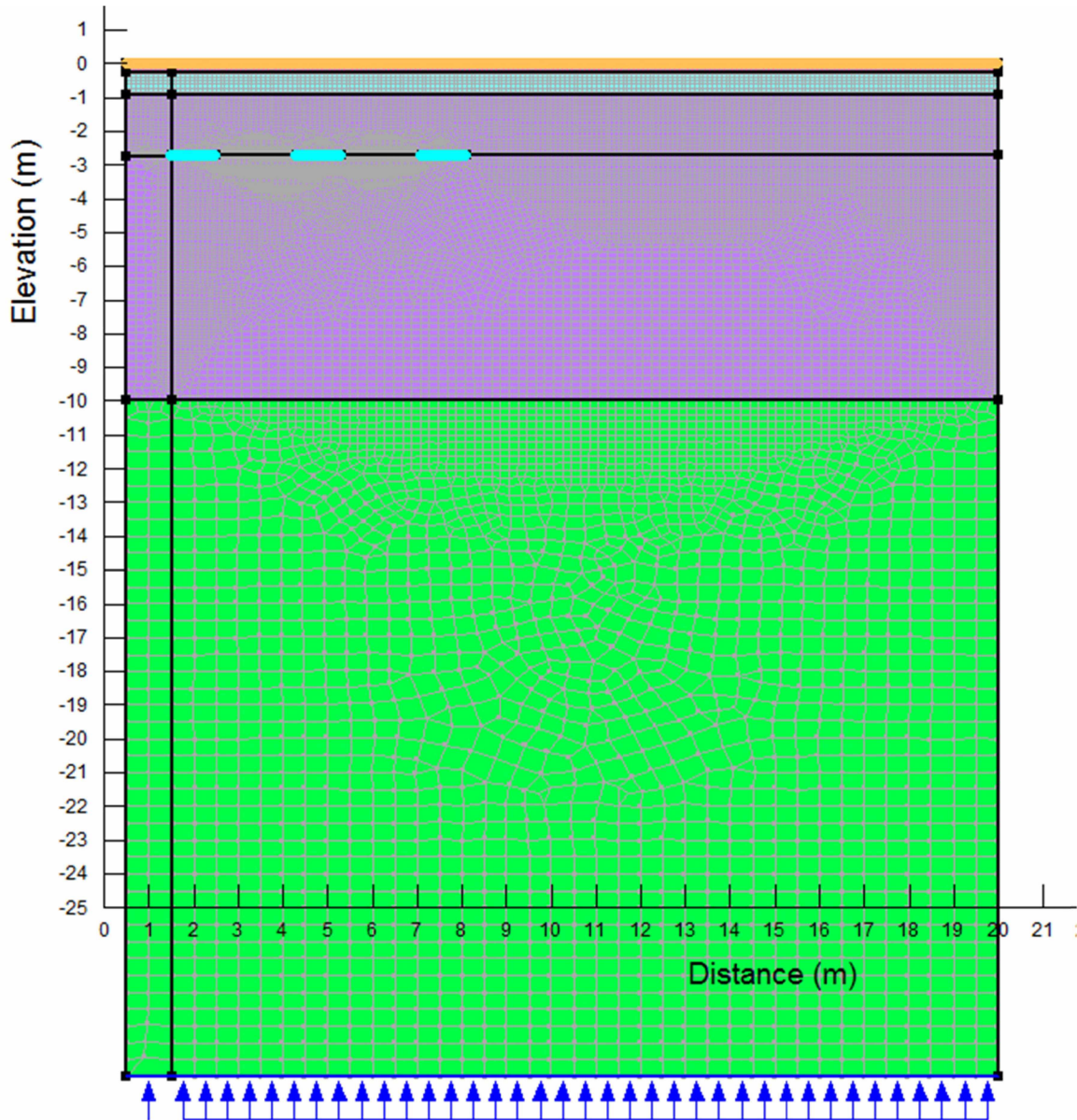

Figure 4.3. Domain and grid layout for the GSHP model. The mesh is the most fine at the surface and around the GHE, which is depicted as the aqua lines at 2.8 m of depths.

4.4 Material Properties

Figure 4.3 also shows the materials used in the model. The soil properties were input using

58

the Temp/W full thermal model. The soil properties are listed in Table 4.1. The thermal conductivity of unfrozen silt comes from the thermal conductivity test that CCHRC performed at the beginning of this project. All the other properties in Table 4.1 come from Romanovsky and Osterkamp's article on the effects of unfrozen water [6] which shares data from the University of Alaska Fairbanks Farm. The UAF farm is less than 1 km from the GHE and in the same cleared field.

Table 4.1. Soil Material Properties.

	Thermal Conductivity (kJ/(day·m·°C)) vs. Temperature (°C)		Unfrozen water content (m³/m³) vs. Temperature (°C)		Frozen volumetric heat capacity (kJ/m²·°C)	Volumetric Water Content (m³/m³)	Unfrozen volumetric heat capacity (kJ/m²·°C)
Frozen Silt (green in Figure)	**K** 112.32 190.08	**T** -0.5 0.5	**UNFWC** 0.017 0.018 0.019 0.021 0.024 0.029 0.12 0.46	**T** -12 -10 -8 -6 -4 -2 -0.02 -0.0002	2,900	2,000	0.41
Unfrozen Silt (purple)	**K** 95.04 122.62	**T** -0.5 0.5	**UNFWC** 0.017 0.018 0.019 0.021 0.024 0.029 0.12 0.46	**T** -12 -10 -8 -6 -4 -2 -0.02 -0.0002	2,900	2,000	0.285
Silt (aqua)	**K** 95.04 122.62	**T** -0.5 0.5	**UNFWC** 0.017 0.018 0.019 0.021 0.024 0.029 0.12 0.46	**T** -12 -10 -8 -6 -4 -2 -0.02 -0.0002	1,900	1,500	0.24
Peaty Silt (pink)	**K** 69.12 120.96	**T** -0.5 0.5	**UNFWC** 0.017 0.017 0.018 0.018 0.019 0.020 0.032 0.051	**T** -12 -10 -8 -6 -4 -2 -0.02 -0.0002	1,500	1,300	0.12

The GHE loops in the model are a simplified thermal model based on the methanol/water heat transfer fluid. Unfrozen thermal conductivity is 44 kJ/ (day·m·°C)); frozen thermal conductivity is 42 kJ/ (day·m·°C)); volumetric heat capacity is 2,000 kJ/m^2°C.

4.5 Boundary Conditions

There are 3 boundary conditions in this model: the geothermal gradient at the bottom, the surface, and the heat extraction from the GHE pipes. The geothermal gradient is based on Goering's 2000 Temp/W model of Thompson Dr.; it is a constant 5.2 kJ/day/m (translated for the 2-dimensional model) [7].

The surface temperature condition uses the actual surface data from the heat pump. Ground surface temperatures in 6 locations across the GHE were collected hourly for the first 4 years of the project. Those hourly temperatures were averaged for each day of the year across all four years (Figure 4.4). The recorded data provides a better estimate of temperatures at the surface because the effect of snow cover is already accounted for.
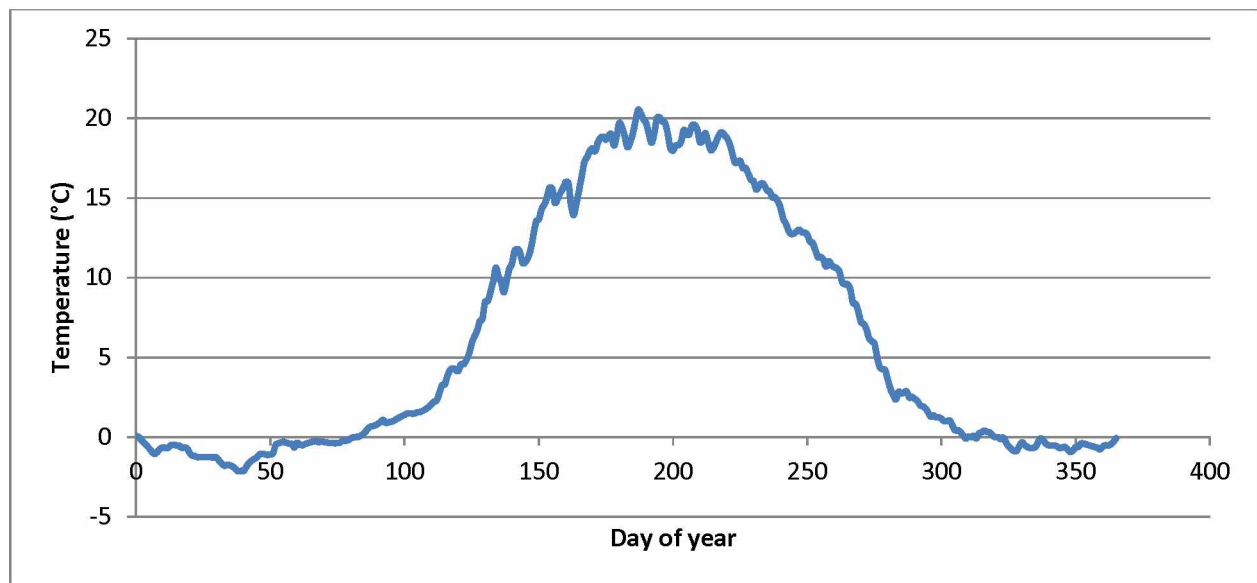
Figure 4.4. GHE surface temperature averages. These data points were under a dusting of soil so they were protected from surface activities.

The heat extraction boundary condition was much more difficult to model. The amount of energy extracted from the ground is quantified but turning it into a 2-D extraction equation either allowed too much cooling in the ground or created no cooling. In order to get a better extraction equation, the median fluid temperature in the GHE slinky coils was used (see Figure 4.5).

60

Figure 4.5. Temperature curve for heat extraction. The temperature of the fluid when the system was not running was assumed to be the same as the surrounding soil.

4.6 Model Correlation

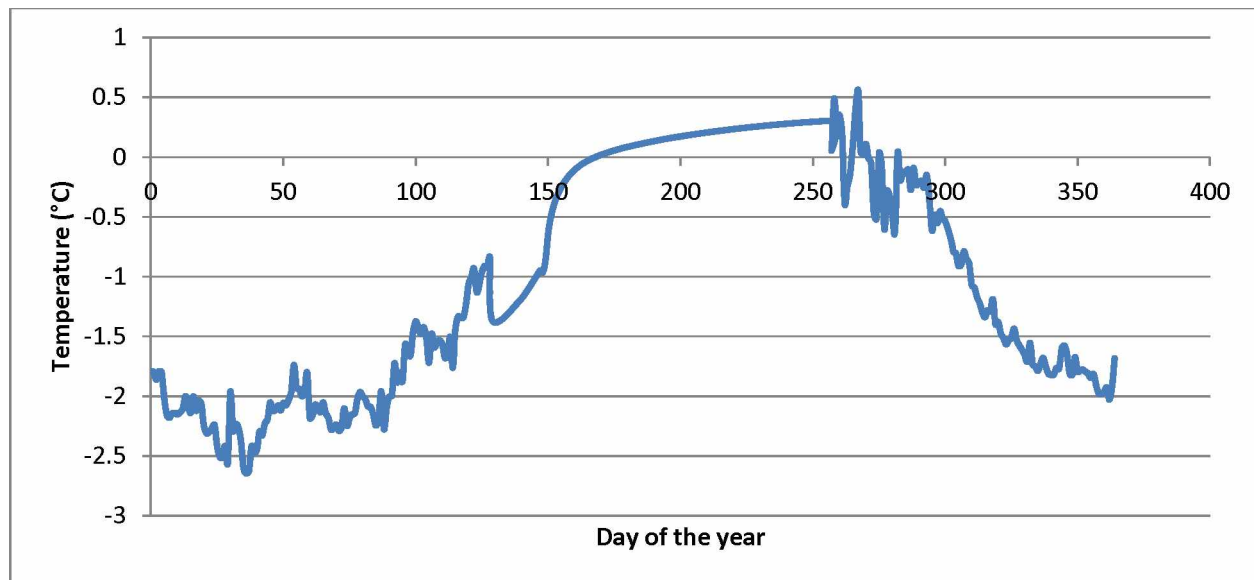A steady state parent model was created using the known temperatures and permafrost depth when the ground loop was installed. The transient analysis was run for 12 years initially, to create a model that demonstrates the actual conditions of the soil. Since the model does not include water movement, the first four years of the soil data were used to evaluate if the model is close to the actual. Correlation temperatures in the soil come primarily from 2 thermistor strings; one in the center of the GHE and one 4 m west of the GHE. Each point only has one sensor and some of the sensors have failed and been replaced, so the data is not as precise as one would want.

A sample of model data outside of the effects of the GHE was compared to the baseline data collected 4 m to the west of the GHE. The baseline sensors have had some water infiltration so the 2015 data was used in order to have more data points to compare. The baseline sensors only reach to 3.7 m below the surface. The data near the surface correlates well (Figure 4.6). Deeper temperatures from the area outside the GHE are colder than the model and have a cold bulge right below the depth of the GHE. It would seem that the GHE heat extraction is also affecting this area and that the baseline temperature string is not far enough removed from the GHE.

61
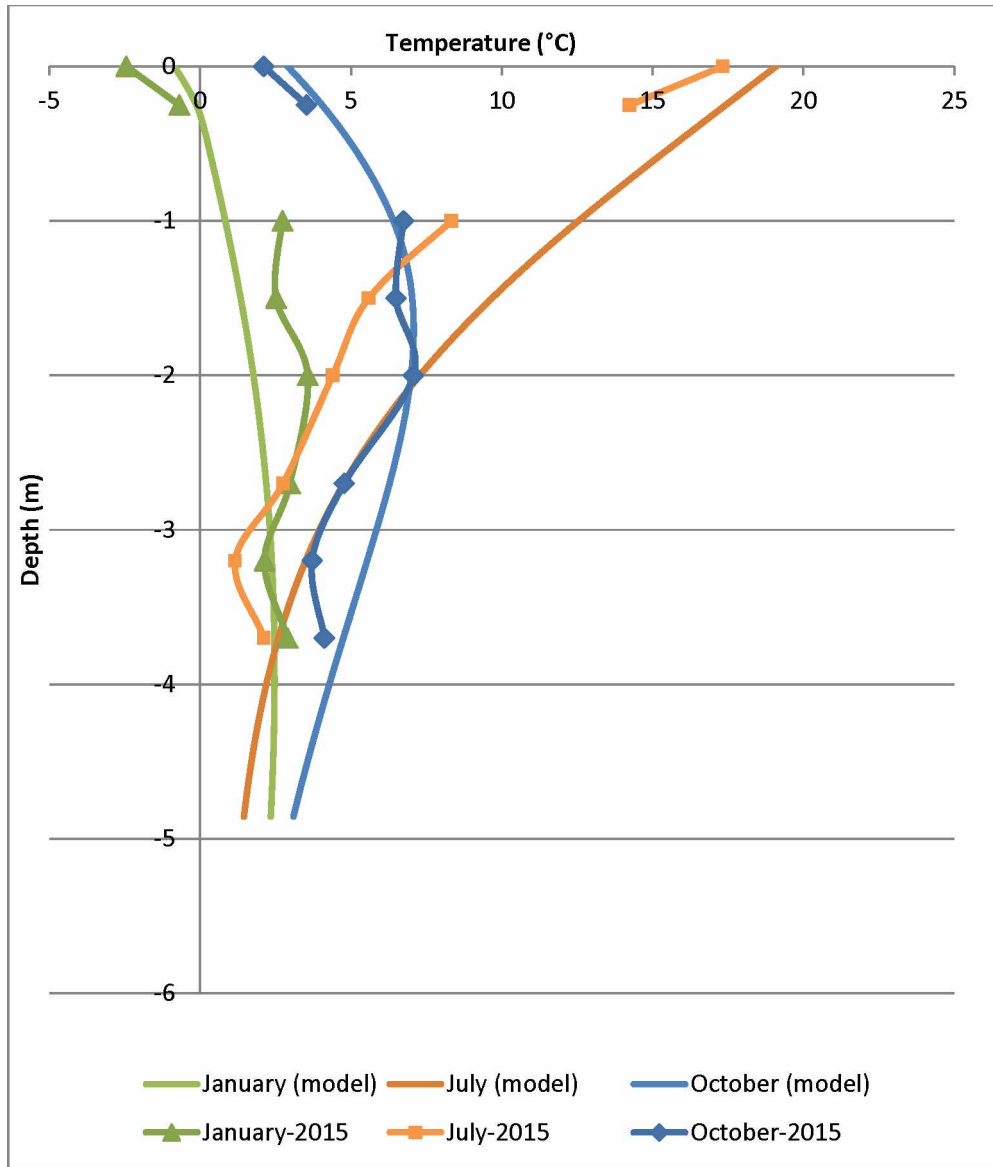
Figure 4.6. Comparison of model data to collected data outside of the GHE. The hole in the collected GHE data is due to a failed sensor at -0.75 m.

The model and the collected data agree within the GHE slightly better above the GHE (Figure 4.7). The coldest spot in the model is right at the level of the GHE (due to the use of fluid temperature as a boundary condition). The coldest spot in that actual GHE is slightly lower than the slinky coils. Below the depth of the GHE the model is much colder (0.4°C) than the measured temperature (2.2°C), this is most likely an indication that the soil properties in the model need to be tweaked further.
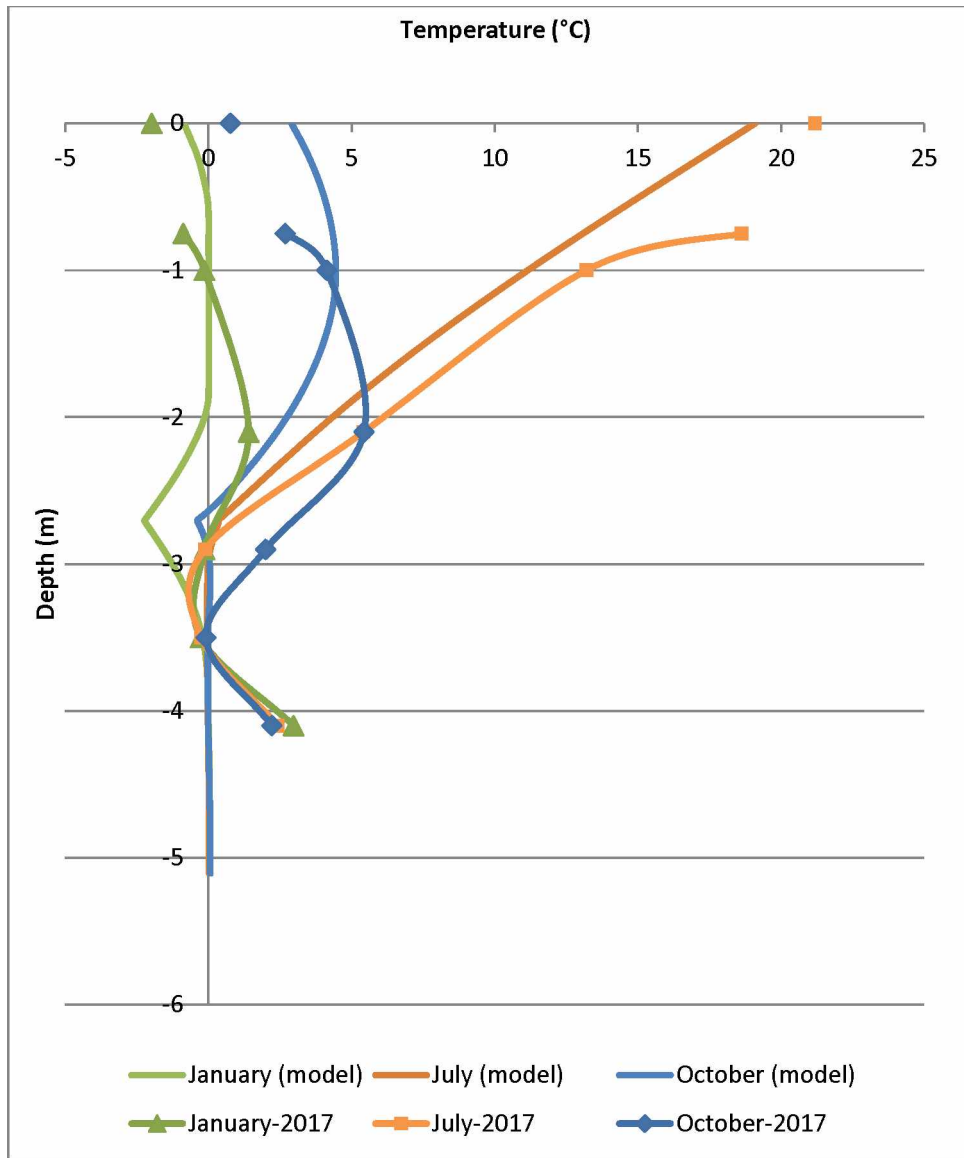
Figure 4.7. Comparison of model data to collected data from the center of the GHE. The sensor at -0.25 m failed in the GHE string.

The frozen soil in the model correlates somewhat with the permafrost tubes through June. Figure 4.8 shows the frozen soil around one of the center slinky coils in the GHE. The soil is frozen down to 3.8 m into June. The permafrost tubes are slender tubes filled with water that extend into the soil. They are pulled out of the soil once a month and checked for ice; the action of exposing them to warm summer temperatures affects their state and it is unknown if they are accurately depicting the soil state after the June check. Figure 4.9 shows the graphical results of the model in June 2017. The model is slightly colder than the actual GHE but the frozen areas in the model are smaller than the actual GHE.
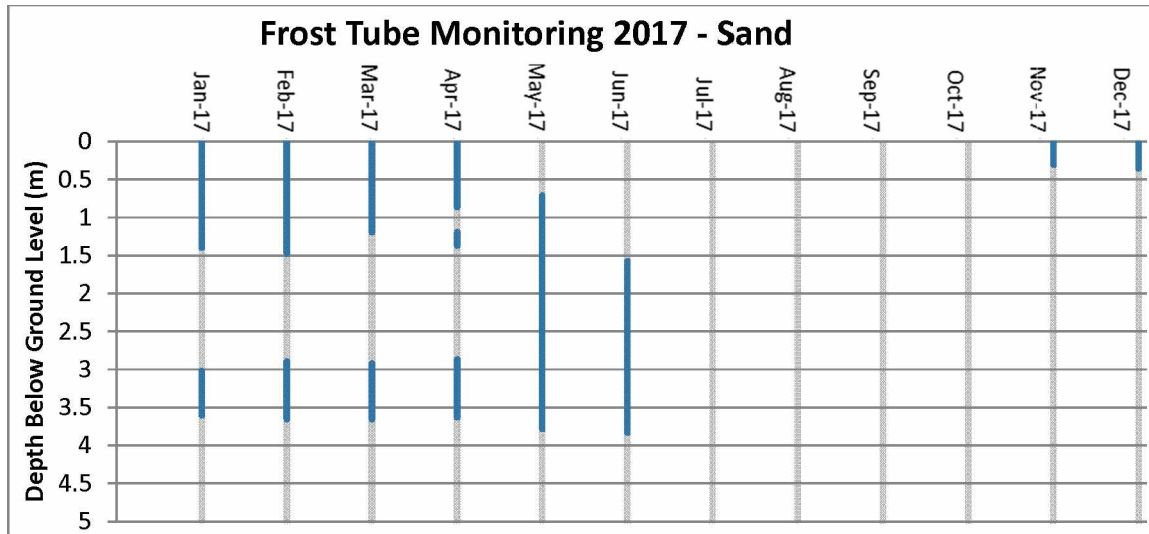
Figure 4.8. Frozen soil in 2017. Freezing data is suspect after the June 2017 check because when the tube is pulled from the soil for analysis all the ice in it thaws. It may be so close to the thaw point that is does not freeze again until the next winter.
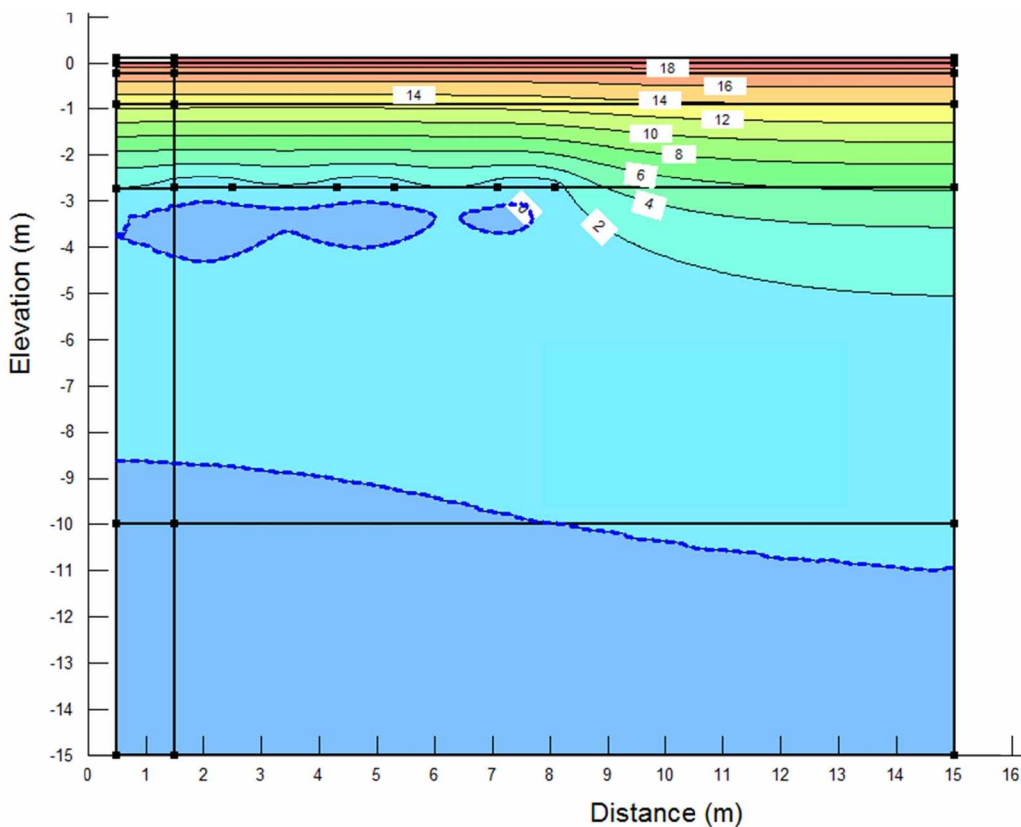
Figure 4.9. The model isotherms in June of year 4. The blue dashed line is the freezing line. The dots at -2.8 meters delineate three slinky coils.

The readings from the permafrost tubes are in question because the temperature in the center of the GHE at 3.5 m below the surface was below freezing from December 2016 until October

2018, as shown in Figure 4.10. The temperature at 3.5 meters below the surface at the center of the GHE seems to demonstrate a strong correlation with the modeled data within 1°C.

Figure 4.10. Measured temperature in the center of the GHE at 3.5 m below the surface. The above freezing temperature in October 2018 means this soil cannot be categorized as permafrost yet.

4.7 Results

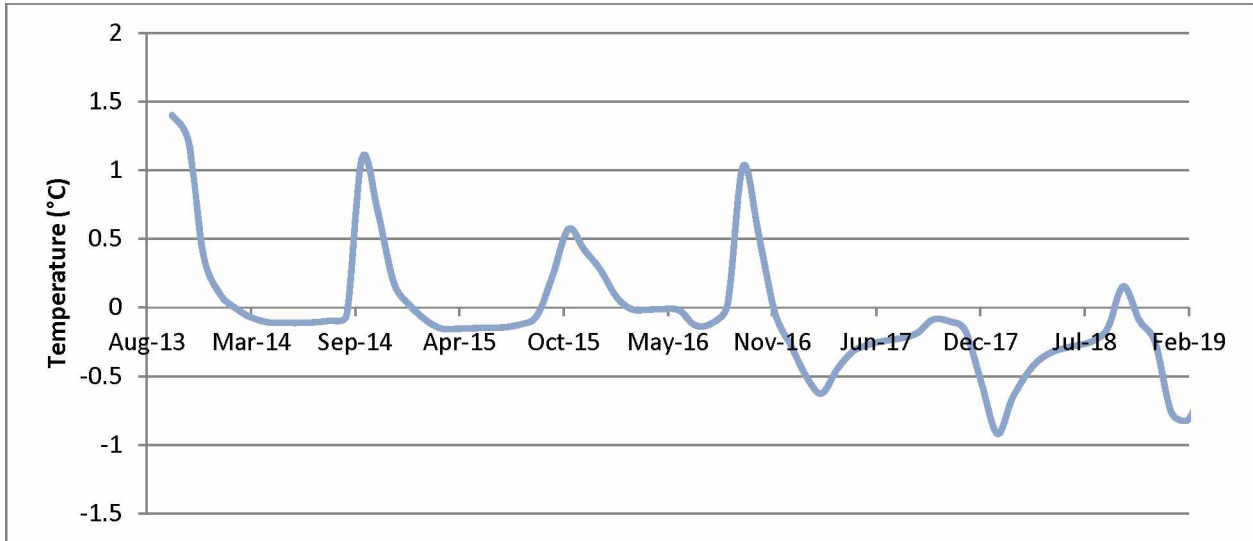The heat pump model was run over a 30 year period to study if the heat pump is viable in a marginal Fairbanks location without the influence of ground water. The life of a heat pump is about 15 to 20 years but the GHE can last at least 50 years [8]. Thirty years seems like a feasible amount of time for a system to operate (a replacement heat pump can utilized the same GHE [9]).

The 30 year model produces interesting results. The amount of ice in the soil increases around and under the GHE for the first 10 to 13 years, however the deep permafrost after rising for a few years starts to thaw away from the GHE (as it has been on the site for 60 years [10]). Figure 4.11 shows the temperature gradient at the end of the 30 year model. The deep permafrost layer away from the GHE was at 10 m at the start of the model, it dropped 10 m in the 30 year model.

The site has been losing permafrost at a rate of about a meter every 9 years, based on data from a borehole near the CCHRC building. The permafrost loss in the model is about 3 meters in 9 years, which indicates that the soil properties in the model could be improved. The water content of the soil from Romanovsky and Osterkamp [6] may be too low, especially compared to borings done in 2012 [11].

65
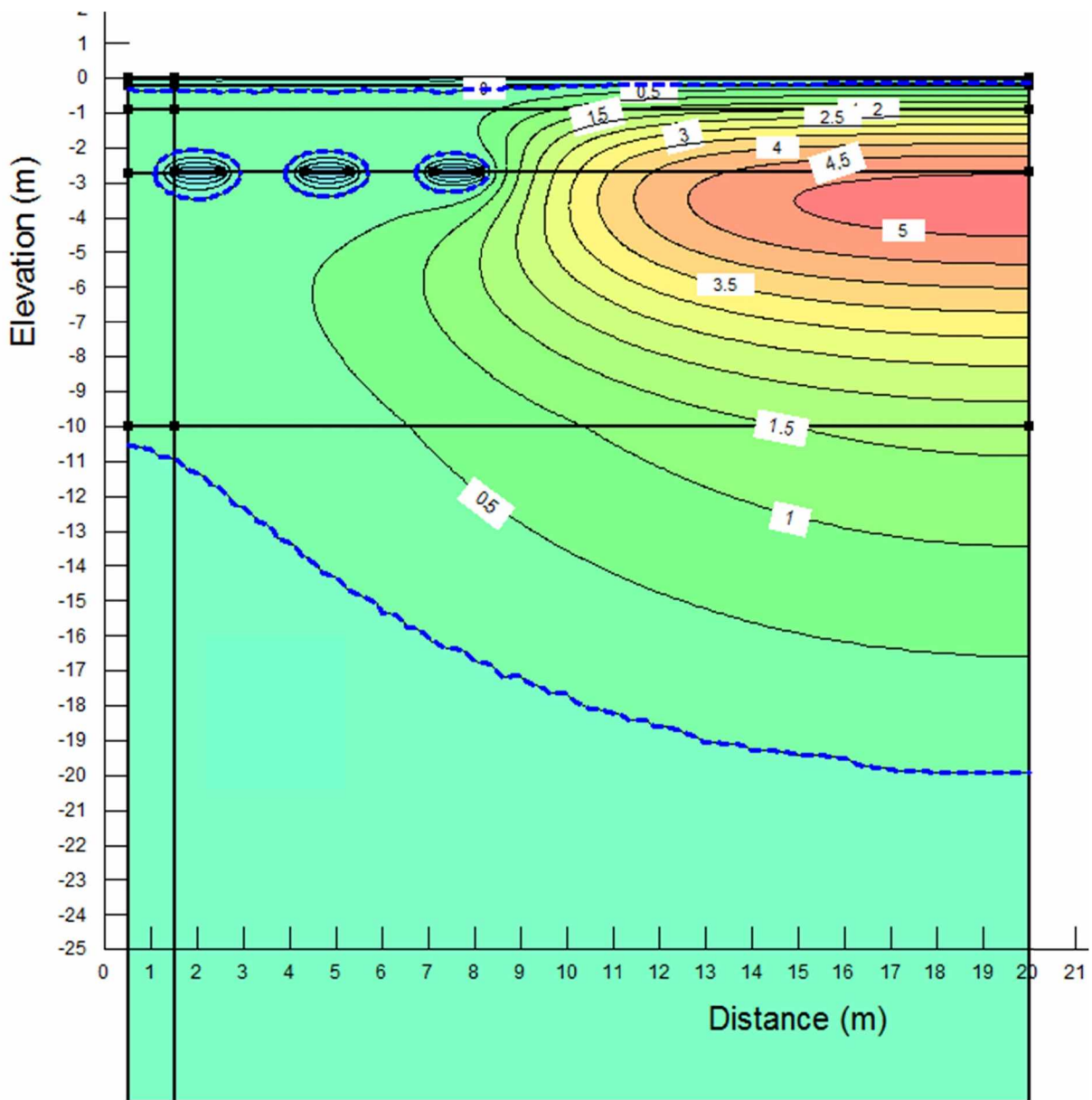
Figure 4.11. Soil temperatures at the end of the 30 year model (in December). Frozen soil that forms around the GHE coils does not last into the next winter.

There are endless tweaks and changes that can go into a model to make it better and more aligned with the physical test. Romanovsky and Osterkamp [6] published the UAF farm data in 2000, the soils have certainly changed since then, now the slinky loops are most likely in soil that is saturated with moving ground water. The ground water is a whole different model that could be added using SEEP/W. However, since this thesis is near its end one more model was attempted using soil moisture data from the 2012 borings [11]. The unfrozen silt and the frozen

silt went from a volumetric water content of 0.285 and 0.41 respectively to 0.53. This resulted in much slower growth of frozen soil in the GHE and less changes to the deep permafrost. However, the deep permafrost table outside of the influence of the GHE still dropped 8 m in the 30 year model (see Figure 4.12).
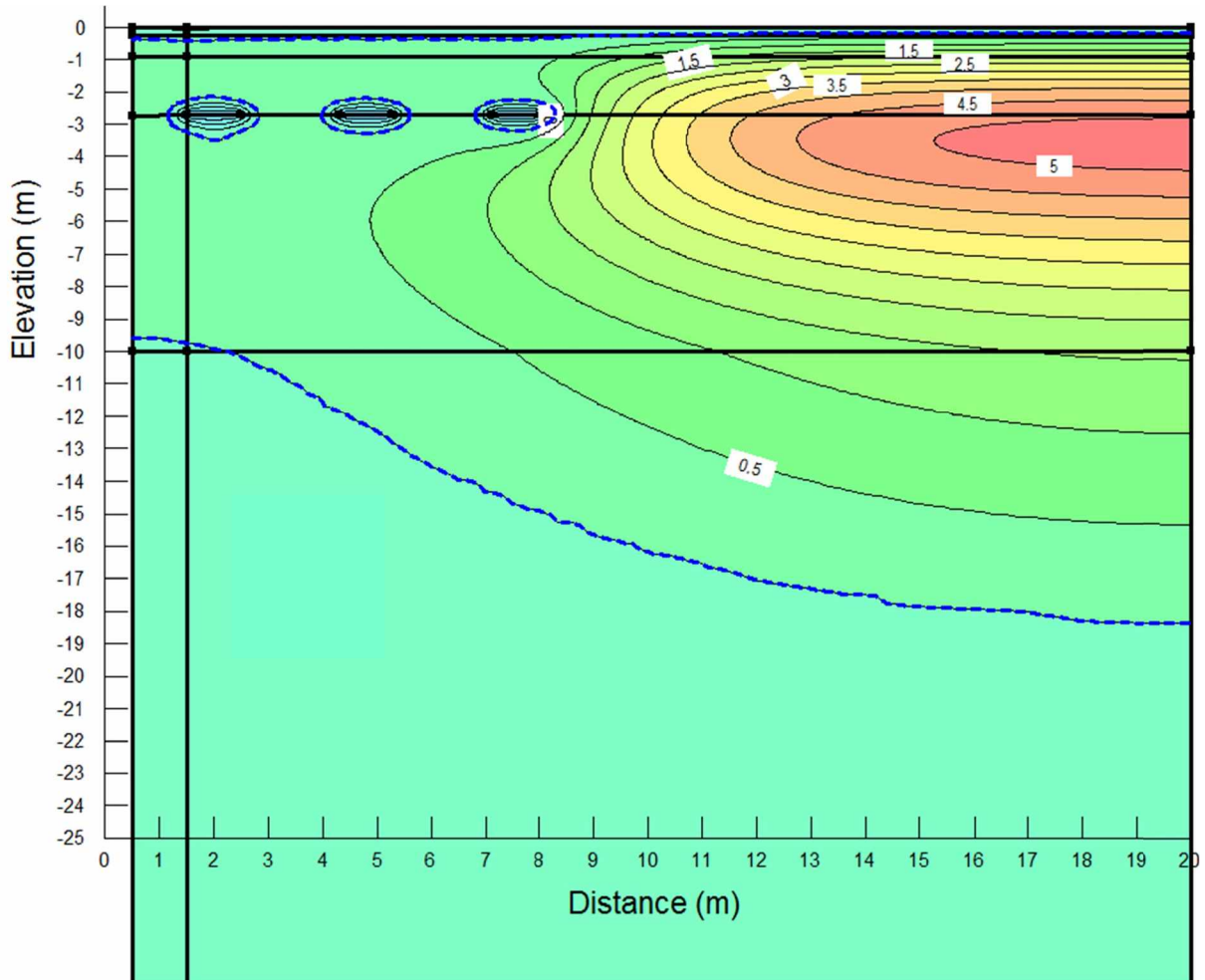
Figure 4.12. Model with higher moisture content at the end of the 30 year model. This at the end of December.

The soil 0.4 m below the GHE began to freeze in the second year of the simulation. In 30 years frozen band grows to a maximum of 2.3 m around the GHE in April of year 10. Subsequent years have a slightly smaller frozen band, which levels out at 2 m in year 24. The frozen band is at its minimum in October at approximately 1.4 m.

4.9 Conclusion

There is certainly more work that could go into the model:

1. Further evaluation of the geothermal gradient

2. Correlate the soil into layers that match recent ground borings better

3. Determine a better heat extraction model based on KJ/day/m not on temperature

4. Add a ground water module

A model with so many parameters has endless possibilities of tweaks. At this point it is hard to determine how realistic the model is 30 years out. The correlations in the first 4 years of data outside the GHE would indicate that the model could be valid, but the quick changes in the deep permafrost table as well as weaker correlation in the GHE center leave some questions.

4.10 Nomenclature

GSHP	Ground Source Heat Pump
CCHRC	Cold Climate Housing Research Center
GHE	Ground Heat Exchanger
q	Heat flux
c_v	Volumetric heat capacity
k	Thermal conductivity
T	Temperature
x	Distance
Q	Applied boundary flux
t	Time
L	Latent heat of water
w	Volumetric water content

4.11 Greek Symbols

λ	Capacity for heat storage

4.12 Subscripts

x	in the x-direction
y	in the y-direction
u	unfrozen

4.13 References

[1]   R. Garber-Slaght, R. Daanen, and A. Roe, "Ground source heat pump efficiency in cold climates," *ASHRAE Trans.*, vol. 120, no. 2, 2014.

[2]   R. Garber-Slaght, C. Craven, R. Peterson, and R. Daanen, "Ground source heat pump demonstration in Fairbanks , Alaska," Cold Climate Housing Research Center, Fairbanks, AK, 2017.

[3]   S. Bishop, "Analysis of ground source heat pumps in sub-Arctic conditions," an M.S. Project, Univeristy of Alaska Fairbanks, 2014.

[4]   R. Garber-Slaght and R. Peterson, "Can ground source heat pumps perform well in Alaska?," in *Proceedings of the IGSHPA Technical/Research Conference and Expo 2017*, 2017.

[5]   GEO-SLOPE International Ltd, *Thermal Modeling with TEMP/W : An Engineering methodology*, no. June. Calgary, Alberta, Canada, 2013.

[6]   V. E. Romanovsky and T. E. Osterkamp, "Effects of unfrozen water on heat and mass transport processes in the active layer and permafrost," *Permafr. Periglac. Process.*, vol. 11, no. 3, pp. 219–239, 2000.

[7]   D. Goering, "Case history passive cooling of permafrost by air convection." 2000.

[8]   J. Meyer, D. Pride, J. O'Toole, C. Craven, and V. Spencer, "Ground-source heat pumps in cold climates," Denali Commission, Fairbanks, AK, 2011.

[9]   T. McFadden, "Supplemental research report on foundation stabilization using a heat pump cooling system at 728 Constitution Drive, Fairbanks, Alaska, USA," Permafrost Techonology Fund, Fairbanks, AK, 2007.

[10]   Shannon & Wilson Inc., "Geotechnial design review proposed UAF/new Geist Road access Fairbanks, Alaska," Alaska Department of Transporation and Public Works, 31-1-01714-001. 2002.

[11]   K. Bjella, "CCHRC Thermal Conductivity Borehole," Cold Climate Housing Research Center, Fairbanks, AK, 2012.

Chapter 5: Thesis Conclusions and Recommendations

5.1 Conclusions

The heat pump at the Cold Climate Housing Research Center (CCHRC) is in a climate that is far colder than any ground source heat pump (GSHP) that has been studied to date. The severe cold coupled with no summer cooling load, and frozen soils create an extreme test of the GSHP technology. The CCHRC heat pump is just one of approximately 50 in the Fairbanks area [1]. A 2014 survey of GSHP owners found them to be satisfied with their systems and the owners felt that their GSHP systems were functioning well [1]. While the CCHRC heat pump is functioning well, with a COP above 2.5 for most of its first 4 years of operation, there is a trend toward lower COPs. Additionally, the cost of operating the GHSP is higher than running a high efficiency boiler, mainly due to variation in the price of oil.

Multiple computer simulations of the GHSP expected the system would equilibrate in the first 5 to 7 years of operation [2], [3]. This thesis ends with the data in year 4, due in part to the rebound in COP in year 5. There is a possibility that the heat pump itself suffered from lower efficiency due to an undiscovered break down of the thermostatic expansion valve (TXV), which may have introduced small parts and dirt into the refrigeration cycle (the TXV failed completely in 2018). At this point there is some uncertainty in the data from years 3, 4, and 5 for determining a trend. Analysis of year 6 data is necessary before a trend can be analyzed.

Even with two years of relatively low COP the heat pump still functions well in the Fairbanks climate. GSHPs have the potential to be a viable source of space heating for Interior Alaska. Further adoption will depend on the price of oil versus the cost of electricity and lowering of the installation costs.

However, the application of nanofluids to this particular GHE is not viable. The fast turbulent flow that is necessary to drive the heat pump lowers the efficacy of the nanoparticles in heat transfer.

The Temp/W model using actual ground loop surface data produced similar outputs to two of the Comsol models in the first 10 years, however when the model was extended to 30 years there are drastic changes to the field away from the influence of the GHE. Using the actual GHE data eliminates the estimates in surface temperature that are inherent in the Comsol models. The Comsol models also used 30-year average air temperature data while the Temp/W model uses a

set of data from 4 years. It is possible that the rapid changes in the temperatures in Alaska are muted in the 30-year data and permafrost thaw in Interior Alaska may speed up that drastically.

The GHE in the Temp/W model does not affect the soil as much as expected from earlier models. There is a small area of frozen soil that develops around the slinky coils but it does not grow larger every year. It may even be shrinking at the 30 year mark. The actual GHE is not creating that much frozen soil either; however, the changes in the groundwater may be having an effect on frozen soils.

5.2 Recommendations for Future Research

5.2.1 Cold Climate Heat Pump

The CCHRC GSHP project grew out of the recommendations that Meyer et al. [4] proposed in their 2011 study. They proposed 7 research topics on GSHPs one of which was to evaluate the long term performance of heat pump and any thermal degradation due to the imbalanced heat extraction of a heat pump. The GSHP at CCHRC has been operational for six heating seasons. The research project was intended to run for at least 10 seasons, approximately ½ the expected life of the heat pump itself. Evaluating the data from years 5 and 6 is necessary as is monitoring the system for at least 4 additional years. The information from these additional years will help determine the long term viability of ground source heat pumps in the Fairbanks climate. Additionally, that data can be used to determine when the GSHP reaches equilibrium in the soil where its efficiency no longer degrades.

The soil conditions around the GHE have changed in the past 6 years, and the ground water may be causing changes to the function of the heat pump. The ground water in the area around CCHRC has risen dramatically in the past 4 years and there is a suspicion that the slinky coils are now laying in moving ground water. This ground water would maintain a temperature slightly above freezing all year long. It would also enhance the thermal conductivity around the slinky coils. Any future analysis of the heat pump will need to account for the changes in ground water.

Meyer et al. [4] also proposed an evaluation of the necessity of a hybrid GSHP that would have some sort of active recharge of the heat in the soil during the summer. Solar thermal recharge is often used and recommended for imbalanced systems in heating dominated climates. Further analysis of the CCHRC heat pump should include a study of the necessity of hybridizing the GHE with solar thermal.

The fall and rise of the efficiency of the heat pump between years 4 and 5 is a mystery. Further analysis of the year 6 electrical data prior to the October 2018 failure of the heat pump itself may shed some light on what happened in year 4. There are other documented system problems which may have also occurred in year 4. An evaluation of the three circulation pumps' power in year 4 might show that the system did not have the proper pumping power that year. The heat pump runs on power from the local grid and does not have any power conditioning. If the data is available it might be worthwhile to look at the power delivered to the whole building for years 4 and 6 to see if there were power surges that could have caused problems with the heat pump electronics or if there were changes in parameters such as voltage and frequency possibly affecting the heat pump performance.

5.2.2 Nanofluids in the Heat Pump

While the nanofluids do not pencil out in the GHE they have the potential to work on the delivery side of a heating system. If they can deliver higher heat with lower temperatures then they can help improve heat plant efficiency. High efficiency boilers and heat pumps deliver lower temperature fluid to a building. Buildings with baseboard heat delivery systems require fluid that is around 70°C in order to deliver enough heat energy. A heat pump or condensing boiler delivers a maximum of 43°C efficiently so it is difficult to install one of these more efficient heating devices in a baseboard building. Could nanofluids be used to enhance the heating capacity of the baseboard so that more efficient low temperature heating systems can be used with baseboard delivery systems?

5.2.3 Finite Element Model of the Ground Heat Exchanger

Finite element modeling is a powerful tool that will continue to be used in this project. As the ground water changes the original question of if the GHE creates permafrost may no longer be relevant. The model could help determine if the system would create permafrost in similar soils with no ground water.

In order to achieve this, the model should be refined. The Temp/W heat flow boundary condition could not produce soil conditions anywhere near reality. A better understanding of the calculations used with the heat flow condition would help to create a better heat extraction model. The steady state starting point for this model was difficult to pin down; mainly due to the fact that the site has been changing dramatically for 60 years due to site clearing. Creating better starting conditions using the data from Thompson Dr. and the UAF farm would also improve the

model. Expanding the model deeper and recalculating the geothermal flux would improve the base model as well.

The more refined model could then be altered to evaluate the system in different soils around Fairbanks and different climates around the state. The saturated silt around the CCHRC building will produce different results than the dry schist soils up in the hills around Fairbanks. Different sizes of GHE could also be evaluated; this would help determine the correct amount of piping a cold climate heat pump requires. Current practice is to oversize the GHE [5] in cold climates to alleviate the problems created by the thermal imbalance. The model could help refine the process of over sizing the GHE; which could save installation costs.

The effects of ground water could also be added to the model. Flowing ground water would enhance the heat transfer around the GHE. It will also elevate the temperature to just above the freezing point, potentially improving the COP of the heat pump. Understanding the GHE improvements from flowing ground water could also allow for smaller GHEs.

5.3 Nomenclature

CCHRC   Cold Climate Housing Research Center

GSHP   Ground Source Heat Pump

COP   Coefficient of Performance

TXV   Thermostatic Expansion Valve

5.4 References

[1]   R. Garber-Slaght and V. Stevens, "Ground source heat pumps in Interior Alaska lessons learned from installed systems," Cold Climate Housing Research Center, Fairbanks, AK, 2014.

[2]   R. Garber-Slaght, R. Daanen, and A. Roe, "Ground source heat pump efficiency in cold climates," *ASHRAE Trans.*, vol. 120, no. 2, 2014.

[3]   R. Garber-Slaght, C. Craven, R. Peterson, and R. Daanen, "Ground source heat pump demonstration in Fairbanks , Alaska," Cold Climate Housing Research Center, Fairbanks, AK, 2017.

[4]   J. Meyer, D. Pride, J. O'Toole, C. Craven, and V. Spencer, "Ground-source heat pumps in cold climates,"Denali Commission, Fairbanks, AK, 2011.

[5]   T. You, W. Wu, W. Shi, B. Wang, and X. Li, "An overview of the problems and solutions of soil thermal imbalance of ground-coupled heat pumps in cold regions," *Appl. Energy*, vol. 177, pp. 515–536, 2016.